iScience

CellPress
OPEN ACCESS

Article

The role of protease-activated receptor 1 signaling in CD8 T cell effector functions

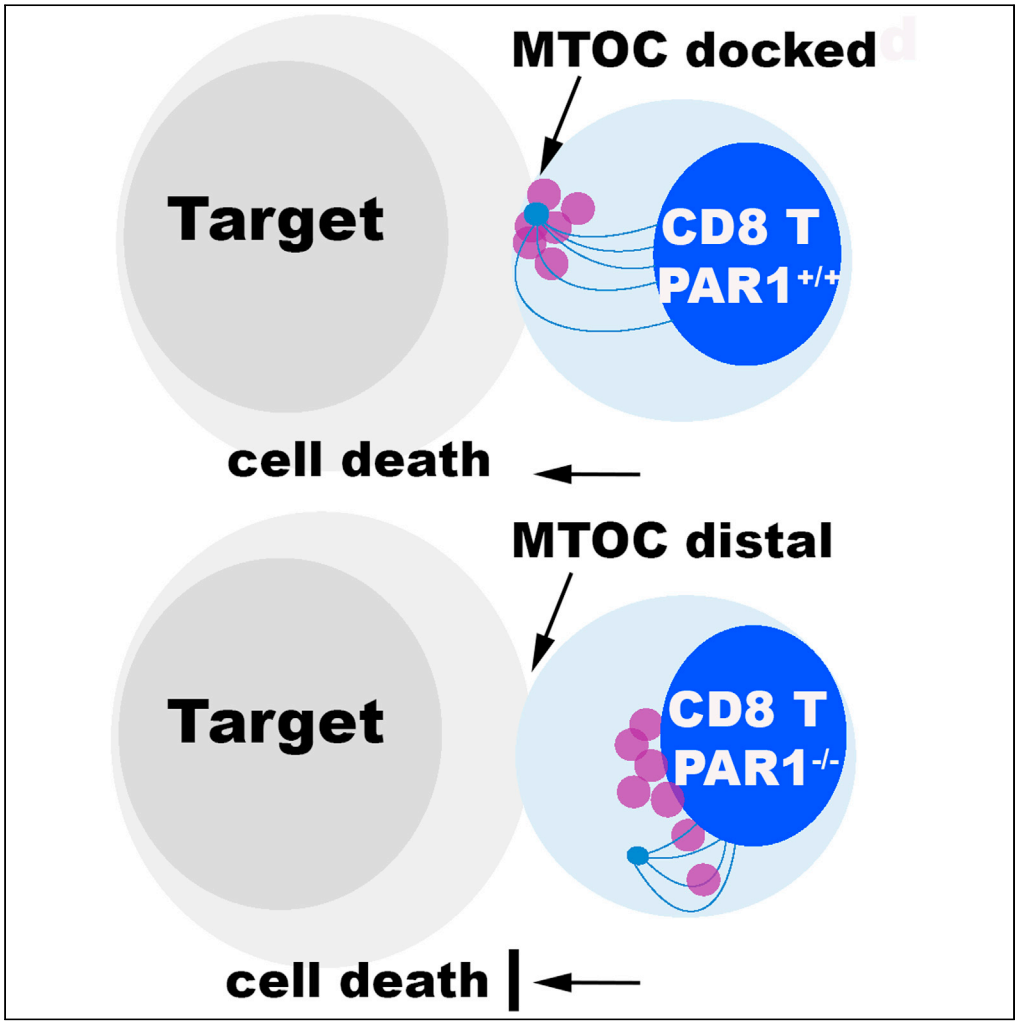

Hui Chen, Mindy Smith, Jasmin Herz, ..., Tatiana Karpova, Dorian B. McGavern, Marta Catalfamo

mc2151@georgetown.edu

Highlights

PAR1 signaling in human CD8 T cells accelerates TCR-induced calcium mobilization

PAR1 participates in the repositioning of the MTOC at the immunological synapse

PAR1 facilitates polarized secretion of cytotoxic granules at the immunological synapse

$PAR1^{-/-}$ Gp33-specific CD8 T cells show reduced expansion and effector function

Chen et al., iScience *24*, 103387
November 19, 2021
https://doi.org/10.1016/j.isci.2021.103387

iScience

CellPress
OPEN ACCESS

Article

The role of protease-activated receptor 1 signaling in CD8 T cell effector functions

Hui Chen,[1,2,7] Mindy Smith,[2,7] Jasmin Herz,[3,8] Tong Li,[1] Rebecca Hasley,[2] Cecile Le Saout,[2] Ziang Zhu,[1] Jie Cheng,[1] Andres Gronda,[4] José A. Martina,[5] Pablo M. Irusta,[4] Tatiana Karpova,[6] Dorian B. McGavern,[3] and Marta Catalfamo[1,9,*]

SUMMARY

CD8 T cells are essential for adaptive immunity against viral infections. Protease activated receptor 1 (PAR1) is expressed by CD8 T cells; however, its role in T cell effector function is not well defined. Here we show that in human CD8 T cells, PAR1 stimulation accelerates calcium mobilization. Furthermore, PAR1 is involved in cytotoxic T cell function by facilitating granule trafficking via actin polymerization and repositioning of the microtubule organizing center (MTOC) toward the immunological synapse. *In vivo*, PAR1$^{-/-}$ mice have reduced cytokine-producing T cells in response to a lymphocytic choriomeningitis virus (LCMV) infection and fail to efficiently control the virus. Specific deletion of PAR1 in LCMV GP33-specific CD8 T cells results in reduced expansion and diminished effector function. These data demonstrate that PAR1 plays a role in T cell activation and function, and this pathway could represent a new therapeutic strategy to modulate CD8 T cell effector function.

INTRODUCTION

CD8 T cells are the main players in cell-mediated immunity against viral infections (Kaech and Cui, 2012; Zhang and Bevan, 2011). During acute viral infections, CD8 T cells undergo extensive proliferation and differentiate into effector cells that have the ability to traffic to peripheral tissues and exert effector functions including cytotoxicity and cytokine secretion (Intlekofer et al., 2005; Kaech and Wherry, 2007; Lazarevic and Glimcher, 2011; Pearce et al., 2003). Because of these important properties, CD8 T cells have become one of the major targets of immune intervention in the setting of viral infections and cancer (Waldman et al., 2020).

CD8 T cells mediate cytotoxic function via two distinct mechanisms: the granule exocytosis and the FAS-FASL pathways. Although the FAS-FASL pathway is a ligand receptor interaction that leads to a signaling cascade driving apoptosis of target cells, the granule exocytosis pathway involves the delivery of preformed cytotoxic molecules including perforin and Granzymes A, B, K, and others (Catalfamo and Henkart, 2003; de Saint Basile et al., 2010; Henkart, 1994; Henkart and Catalfamo, 2004; Ju et al., 1994; Lowin et al., 1994; Simon et al., 2000; Smyth et al., 2001). These preformed mediators are stored in lysosome-like compartments or secretory lysosomes and are delivered by the regulated secretion pathway at the immunological synapse (IS) formed by the CD8 T cell and the target cell (Catalfamo and Henkart, 2003; Dieckmann et al., 2016; de la Roche et al., 2013; Stinchcombe and Griffiths, 2007; Stinchcombe et al., 2006; Smyth et al., 2001; Wurzer et al., 2019).

T cell receptor (TCR) recognition of antigenic peptides presented by major histocompatibility complex (MHC) class I molecules leads to the activation of proximal components of the signaling cascade including the linker for activation of T cells (LAT), Lck and ZAP70, all clustering at the center of the IS and forms a domain called the central supramolecular activation cluster (cSMAC) (Grakoui et al., 1999; Monks et al., 1998; Varma et al., 2006; Yokosuka et al., 2005). The cSMAC is surrounded by a peripheral SMAC (pSMAC) formed by receptor-ligand interactions of adhesion molecules LFA1-ICAM1 and the cytoskeletal protein talin. Next to the pSMAC, F-actin accumulates in the distal SMAC (dSMAC) zone, giving the appearance of a "bull's-eye" conformation. The delivery of cytotoxic granule contents occurs in a polarized fashion at the secretory domain, a region localized at the pSMAC and proximal to the cSMAC (Potter et al.,

[1]Department of Microbiology and Immunology, Georgetown University School of Medicine, Washington, DC, USA

[2]Laboratory of Immunoregulation, National Institute of Allergy and Infectious Diseases, National Institutes of Health, Bethesda, MD, USA

[3]Viral Immunology and Intravital Imaging Section, National Institute of Neurological Disorders and Stroke, National Institutes of Health, Bethesda, MD, USA

[4]Department of Human Science, Georgetown University, Washington, DC, USA

[5]Cell and Developmental Biology Center, National Heart, Lung and Blood Institute, National Institutes of Health, Bethesda, MD, USA

[6]Laboratory of Receptor Biology and Gene Expression, National Cancer Institute, National Institutes of Health, Bethesda, MD, USA

[7]These authors contributed equally

[8]Present address: Department of Pathology and Immunology, Washington University, St. Louis, MO, USA

[9]Lead contact

*Correspondence: mc2151@georgetown.edu

https://doi.org/10.1016/j.isci.2021.103387

2001; Stinchcombe et al., 2001). The movement and polarized secretion of the cytotoxic granules is facilitated by the repositioning of the microtubule organizing center (MTOC) at the IS (Billadeau et al., 2007; Geiger et al., 1982; Stinchcombe et al., 2001). Ultimately, the secretion of cytolytic molecules inside the infected cell through the synapse cleft induces target cell death (Dustin and Long, 2010; Jenkins and Griffiths, 2010; Stinchcombe and Griffiths, 2007).

We and others have shown that human CD8 T cells express the protease-activated receptor 1 (PAR1, thrombin receptor). PAR1 is a member of the G-protein-coupled protease-activated receptor family. Four members of this family have been identified, PAR1, PAR2 PAR3, and PAR4. In humans, PAR1, PAR3, and PAR4 are activated by thrombin, the main serine protease of the coagulation cascade, whereas in mice PAR3 and PAR4 are the main receptors for thrombin. In addition, PAR2 is activated by trypsin, tryptase, and other coagulation factors (Coughlin, 2000; Ishihara et al., 1998; Kahn et al., 1998; Sambrano et al., 2001; Xu et al., 1998). PAR1 is also expressed by a variety of cells including cells from the innate and adaptive immune systems, linking the immune activation, inflammation, and coagulation pathways (Antoniak et al., 2013, 2017; Bar-Shavit et al., 2002; Chen and Dorling, 2009; Cunningham et al., 2000; Hurley et al., 2013; Khoufache et al., 2013; Le et al., 2018; Lopez et al., 2014; Mari et al., 1994; Mudd et al., 2016; Niessen et al., 2008; Radulovic et al., 2016; Rohani et al., 2010; Scholz et al., 2004; Shpacovitch et al., 2007; Sutherland et al., 2007; Steinhoff et al., 2005). However, its role in T lymphocytes is not well defined. In T cells, thrombin activation of PAR1 induces tyrosine phosphorylation of proximal components of the TCR signaling (Bar-Shavit et al., 2002; Mari et al., 1994). In CD8 T cells, PAR1 activation enhanced TCR-dependent cytokine secretion and T cell movement (Hurley et al., 2013; Mudd et al., 2016).

In contrast to other G-coupled protein receptors, which are activated by receptor-ligand interactions, PAR1 is activated through proteolytic cleavage of its extracellular N-terminal domain, generating a tethered ligand. Binding of this tethered ligand to the body of the receptor induces transmembrane signaling through coupling to heterotrimeric G proteins (Arora et al., 2007; Coughlin, 2000; Heuberger and Schuepbach, 2019; McCoy et al., 2010; Vu et al., 1991; Woulfe, 2005).

PAR1 has been shown to mainly couple to the G protein subfamilies such as Gq and G12/13 proteins. The activation of Gq protein downstream of PAR1 stimulates phospholipase Cβ-mediated phosphoinositide hydrolysis, PKC activation, and calcium mobilization (Coughlin, 2001; Hung et al., 1992). On the other hand, PAR1-induced activation of G12/13 protein leads to Rho kinase activation and phosphorylation of myosin light-chain kinase, promoting cytoskeleton reorganization (Coughlin, 2001; Klages et al., 1999).

PAR1 has been identified as the main receptor for thrombin; however, other proteases that are not associated with the coagulation cascade such as enzymes that are contained in the cytotoxic granules including granzymes can also activate PAR1 (Cooper et al., 2011; Coughlin, 2000; Lee et al., 2017; Sen et al., 2011; Suidan et al., 1994; Wilson et al., 2009). Particularly, it has been shown that Granzyme A, B, and K can activate PAR1 in cells such as neurons and endothelial cells under inflammatory conditions (Cooper et al., 2011; Heuberger and Schuepbach, 2019; Lee et al., 2017; Sharma et al., 2016; Suidan et al., 1994; Wang et al., 2012). However, the cleavage site and the downstream signals of these activators are not well defined.

In the present study, we showed that PAR1 signaling is involved in CD8 T cell cytotoxicity mediated by the granule exocytosis pathway. In addition, PAR1 deficiency in LCMV GP33-specific CD8 T cells resulted in reduced expansion and diminished effector function. These data demonstrate that *in vivo* PAR1 plays an important role in T cell activation, function, and recruitment of effector CD8 T cells in peripheral tissues.

RESULTS

PAR1 expression levels increase with CD8 T cell differentiation

We previously reported that CD8 T cells express PAR1, and its activation by thrombin in combination with TCR stimulation led to increased secretion of IFNγ (Hurley et al., 2013). However, whether PAR1 plays a role in cytotoxic function is not defined. To address this question, we first examined the mRNA expression of other members of the PAR family (PAR2, PAR3, and PAR4), and we found that PAR1 is the main family member expressed in human and murine CD8 T cells (Figure S1A). Because of its potential role in CD8 T cell function, we next study the relationship between the expression of PAR1 and the transcription factors associated with CD8 T cell effector differentiation (T-bet, Eomes), molecules involved in cytotoxic function

including perforin, Granzyme A (GZA), Granzyme B (GZB), and the chemokine receptor CXCR3, which is important for the trafficking of CD8 T cells into peripheral tissues (Buggert et al., 2014; Hu et al., 2011; Hickman et al., 2015; Intlekofer et al., 2005; Kurachi et al., 2011; Lazarevic and Glimcher, 2011; Pearce et al., 2003; Taqueti et al., 2006).

PAR1 expression was measured in resting CD8 T cells from the PBMCs of healthy volunteers (n = 10). PAR1 expression increases with CD8 T cell differentiation, with the lowest levels found on naive ($CD45RA^{+}CD27^{+}$) cells, and the highest in the memory ($CD45RA^{-}CD27^{+}$) and terminal effector memory ($CD45RA^{+}CD27^{-}$) phenotypes (Figure 1A) (Hurley et al., 2013). As expected, similar expression pattern was observed for the transcription factors T-bet and Eomes (Figure 1B) and the effector molecules GZA, GZB, and perforin (Figure 1D) with exception of CXCR3 (Figure 1F) that was expressed by all subsets.

More importantly, PAR1 expression showed to be associated with the expression of T-bet and Eomes (Figure 1C), cytotoxic molecules (Figure 1E), but not CXCR3 (Figure 1G), in resting human CD8 T cells.

These results indicate that PAR1 expression is associated with effector differentiation and potentially plays a role in effector function of CD8 T cells.

PAR1 signaling accelerates TCR-induced calcium mobilization in human CD8 T cells

We have previously shown that PAR1 activation increases IFNγ secretion by CD8 T cells, suggesting that PAR1 enhances TCR signaling (Hurley et al., 2013). In addition, previous studies showed that TCR can engage the GTP-bound α subunit of the heterotrimeric class of G proteins belonging to the Gq family; however, the receptor that bridges these two pathways has not been identified (Bueno et al., 2006; Harnett and Rigley, 1992; Ngai et al., 2008; Stanners et al., 1995).

We next investigated whether PAR1 activation influences TCR signaling. PAR1, when coupled to Gq, involves activation of phospholipase C-beta (PLCβ), promoting rapid calcium mobilization (Coughlin, 2000; Ramachandran et al., 2012; Soh et al., 2010). We first evaluated if PAR1 in human CD8 T cells signals through Gq protein by measuring calcium mobilization by its main activator, the serine protease thrombin. Thrombin at concentrations of 3–300 nM led to a rapid calcium mobilization that was efficiently blocked by the PAR1 antagonist SCH79797 in activated human CD8 T cells (Figure S1B) (Ahn et al., 2000). In addition, stimulation of PAR1 by thrombin was efficiently blocked by the PAR1 antagonists SCH79797 and SCH530348 in activated human CD8 T cells (Figure S1C) (Ahn et al., 2000). Consistent with the mRNA expression (Figure S1A) only the PAR1 agonist peptide induced a calcium response comparable with that induced by the serine protease thrombin. PAR4 and PAR2 agonist peptides showed only a marginal response similar to the peptide control (Figure S1D). These results suggest that human CD8 T cells mainly express PAR1, and its activation signals through Gq protein.

We next evaluated the effect of PAR1 activation in addition to TCR signaling. We found that activation of PAR1 by thrombin accelerated the calcium mobilization triggered by TCR stimulation (Figure 2A).

PAR1 can be activated by other serine proteases including granzymes and other lysosomal enzymes that are present in the cytotoxic granules (Cooper et al., 2011; Lee et al., 2017; Suidan et al., 1994; Wilson et al., 2009). We investigated whether PAR1 blockade attenuates calcium mobilization induced by TCR stimulation (Figure 2B). The PAR1 antagonists SCH79797 and SCH530348 were used at concentrations that efficiently blocked thrombin stimulation in activated CD8 T cells (Figure S1C). We found that PAR1 blockade with the antagonist SCH530348 significantly reduced TCR signaling. In contrast, this effect was not observed with the antagonist SCH79797, suggesting that this antagonist in T cells may have a distinct mode of action (Figure 2B). In addition, the PLC inhibitor U73122 efficiently blocked TCR-induced calcium mobilization, in contrast to the U73343, a close analogue that was used as control (Figure 2B) (Gaud et al., 2018).

Consistent with PAR1 activation, TCR stimulation of CD8 T cells led to a significant reduction of the fluorescence intensity of PAR1 surface staining relative to unstimulated cells (Figure 2D, left panel). In addition, the loss of PAR1 surface staining was associated with the strength of the signal, and 10 μg/mL induced higher loss of PAR1 surface staining than 1 μg/mL of anti-CD3mAb (Figures 2C and 2D, right panel). The

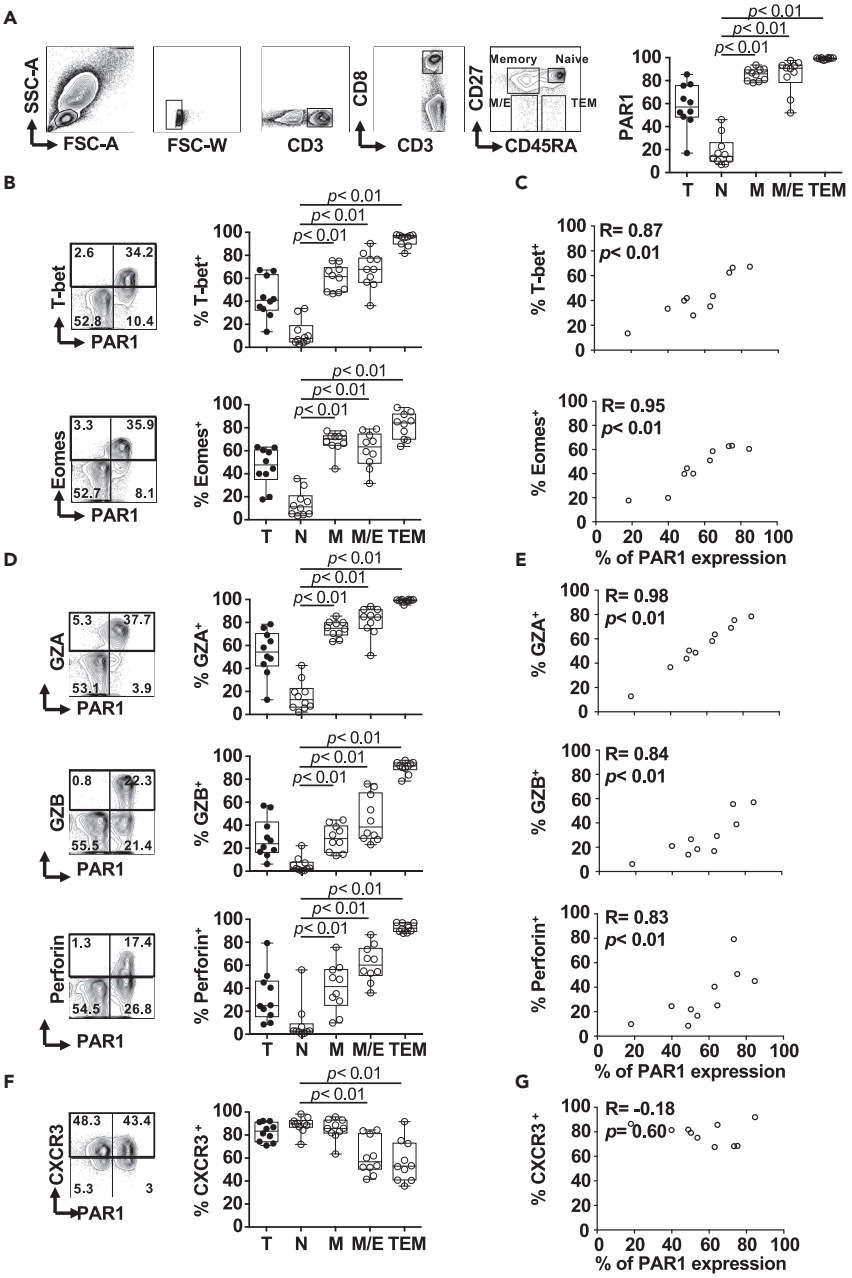

Figure 1. PAR1 expression is associated with CD8 T cell differentiation and cytotoxic potential

PBMC from healthy donors (n = 10) were analyzed for expression of PAR1, T-bet, Eomes, GZA, GZB, perforin, and CXCR3 in CD8 T cells. CD8 T cell subsets were defined as naive (N, $CD45RA^{+}CD27^{+}$), memory (M, $CD45RA^{-}CD27^{+}$), memory/effector (M/E, $CD45^{-}CD27^{-}$), and terminal effector memory (TEM, $CD45RA^{+}CD27^{-}$). Full minus one (FMO) was used as control. Antibodies used were listed in Table 1. (A) Gating strategy and expression of PAR1 in human CD8 T cell subsets.

(B) Expression of transcription factors T-bet or Eomes in CD8 T cell subsets.

(C) Relationship between expression of PAR1 and T-bet or Eomes.

(D) Expression of cytolytic molecules GZA, GZB, and perforin in CD8 T cell subsets.

(E) Relationship between expression of PAR1 and GZA, GZB, and perforin.

(F) Expression of CXCR3.

(G) Relationship between PAR1 and CXCR3 expression. The box and whisker plot showed median value with interquartile range. Statistical analysis was performed using nonparametric paired Wilcoxon test. *p* value <0.05 was considered significant. Nonparametric Spearman analysis was performed to determine the correlation between markers expressions.

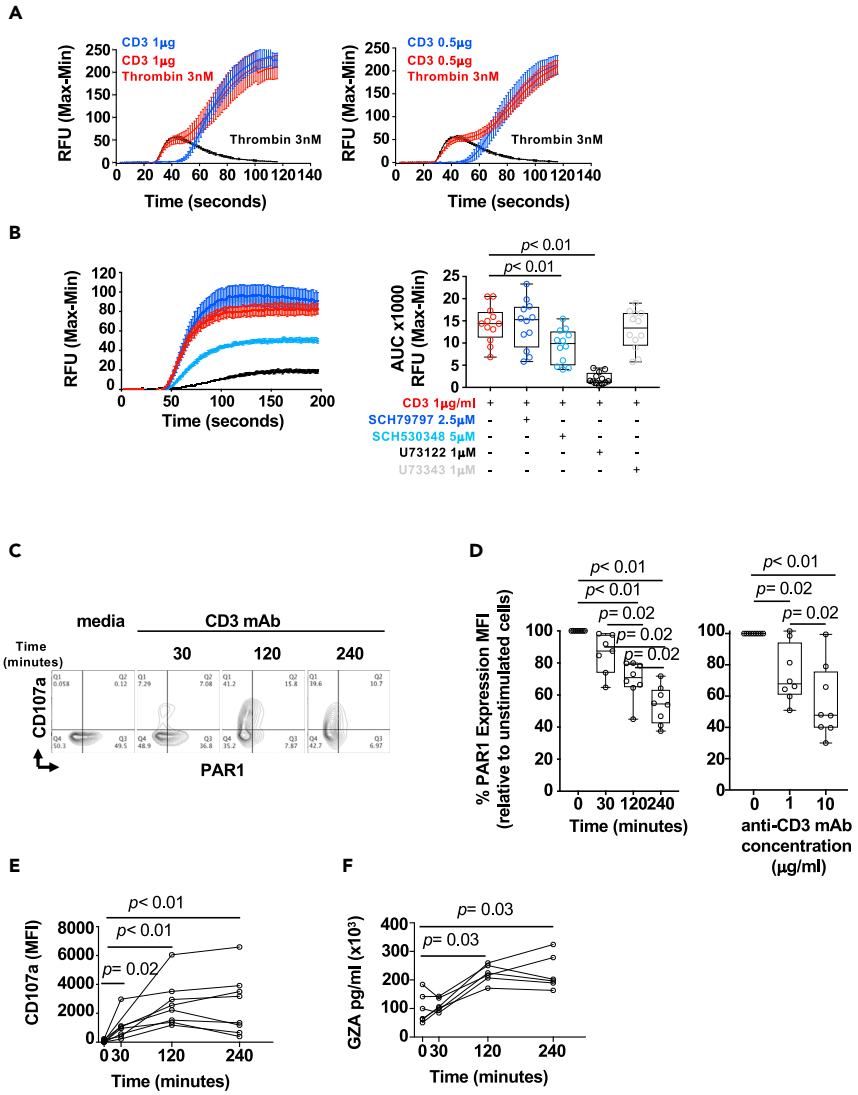

Figure 2. PAR1 signaling cross-talks with TCR-induced calcium mobilization in activated human CD8 T cells

Human CD8 T cells isolated from healthy volunteers were activated with anti-CD3 and anti-CD28 mAbs and expanded in the presence of IL-2 for 11–18 days. Calcium mobilization was measured using FLIPR assay for up to 200 s. (A) Kinetics of TCR-induced calcium flux in response to 0.5 µg/mL and 1 µg/mL CD3 mAbs in the presence or absence of 3 nM thrombin. Representative experiment of (n = 3).

(B) (Left panel) Representative experiment of TCR-induced calcium mobilization in activated human CD8 T cells in response to 1 µg/mL anti-CD3 mAb in the presence or absence of PAR1 inhibitors SCH79797 (2.5 µM) and SCH530348 (5 µM), PLC inhibitor 1 µM U73122, or 1 µM analog control U73343. The graph (right panel) represents the experiments of TCR-induced calcium mobilization with activated CD8 T cells from healthy donors tested (n = 12). Box and whisker plot represent median value with interquartile range. The total area under the curve (AUC) was calculated using GraphPad prism. Comparisons between culture conditions was performed using nonparametric paired Wilcoxon test. *p* value <0.05 was considered significant.

(C) PAR1 surface expression upon TCR stimulation. Activated CD8 T cells from healthy donors (n = 8) were stimulated in media and plate bound anti-CD3 mAb at concentration 10 µg/mL for 30, 120, and 240 min, and PAR1 and CD107a surface expression was evaluated by flow cytometry. Representative contour plots of surface expression of PAR1 and CD107a.

(D) Loss PAR1 surface staining over time of stimulation with 10 µg/mL anti-CD3 mAb during 30, 120, and 240 min (left panel) and stimulation with 1 µg/mL and 10 µg/mL anti-CD3 mAb for 240 min (right panel). The graph represents PAR1 surface staining as the frequency of Mean Fluorescence Intensity (MFI) of the stimulated condition relative to the expression PAR1 (MFI) in the unstimulated condition.

(E) Surface expression of CD107a (MFI) during stimulation with 10 µg/mL anti-CD3 mAb.

(F) Granzyme A was measured in the supernatants of the stimulated cells. Comparisons between culture conditions was performed using nonparametric paired Wilcoxon test. *p* value <0.05 was considered significant.

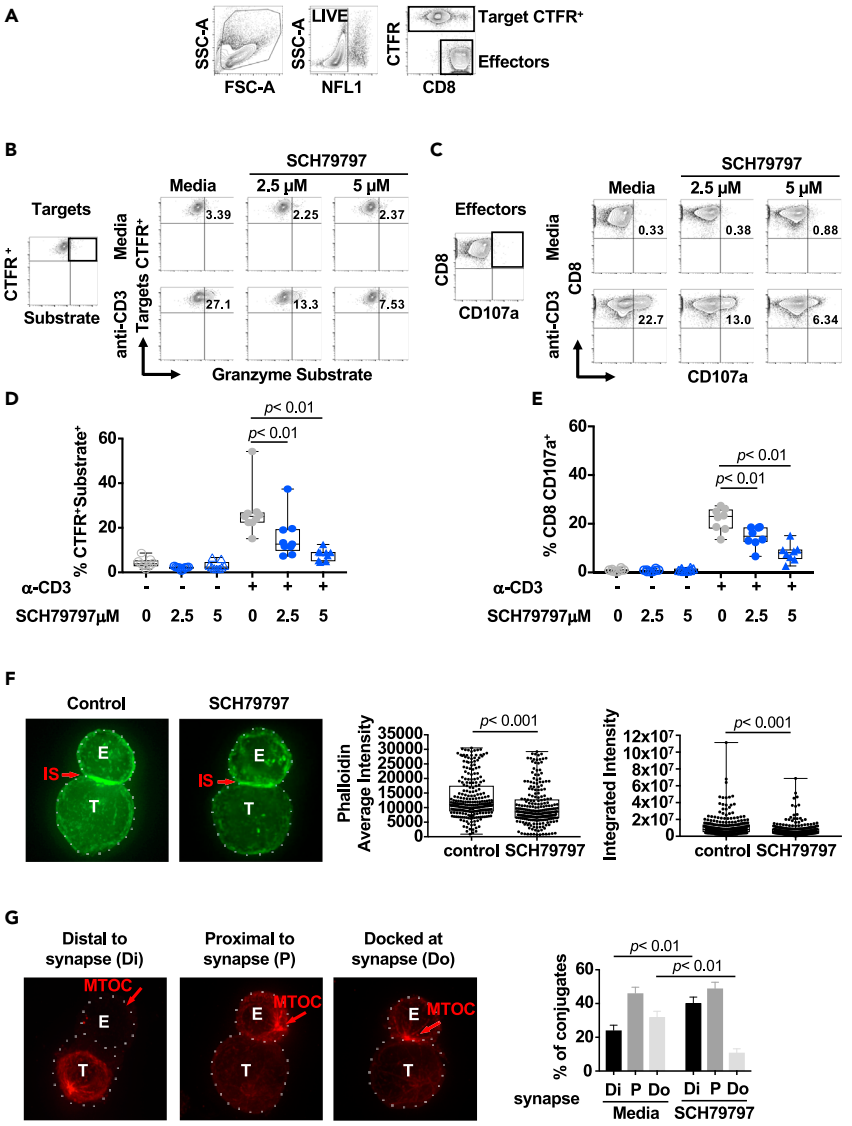

Figure 3. PAR1 blockade in human CD8 T cells inhibits degranulation and cytotoxicity function by reducing MTOC positioning at the IS

Human CD8 T cells from healthy donors (n = 9) were activated with CD3/CD28 for 3 days and followed by expansion for an additional 11–18 days in the presence of rhIL-2. Redirected killing assay was performed using biotinylated L1210 (FAS^-) targets. Target cells were labeled with CTFR. Both effectors and targets were labeled with NFL1 to exclude the dead cells in the flow cytometry analysis. Activated CD8 T cells were preincubated with media or 2.5 μM and 5 μM of the PAR1 inhibitor SCH79797 before mixing with the target cells at 27:1 (E:T ratio) in the presence or absence of 10 μg/mL anti-CD3 and GZB substrate. After 1-h incubation cells were harvested and stained for CD8 and CD107a. (A) Gating strategy to analyze target cells ($CTFR^+$) and effector CD8 T cells.

(B) Targets were analyzed for GZB activity ($CTFR^+Substrate^+$).

(C) Effector CD8 T cells were analyzed for surface expression of lysosomal-associated membrane protein (LAMP-1, CD107a).

(D) Quatitative plot of the effect of PAR1 inhibition by SCH79797 on the granzyme activity ($CTFR^+Substrate^+$) in the targets.

(E) Quantitative plot of the effect of PAR1 inhibition by SCH79797 on CD8 T cell degranulation as indicated by surface CD107a expression. Data are represented with box and whisker plot of median value with interquartile range. Statistical analysis was performed using nonparametric Mann-Whitney test for comparison between groups and nonparametric paired Wilcoxon test for comparisons between conditions. p value <0.05 was considered significant.

(F) Conjugates were prepared using biotinylated L1210 and activated CD8 T cells in the presence of 10 μg/mL biotin-CD3. F-actin accumulation at the immunological synapse (IS) was measured by the average and integrated intensity of

Figure 3. *Continued*
phalloidin staining. The box and whisker plot showed median value with interquartile range (n = 257–263 conjugates of each group).
(G) Conjugates were stained with antibodies against alpha-tubulin (red) to visualize the microtubule-organizing center (MTOC). Quantification of MTOC polarization was expressed as distal (Di), proximal (P), and docked (Do) to the IS. Data are pooled from three independent experiments (n = 185–190 conjugates of each group).

loss of surface staining of PAR1 occurs during CD8 T cell degranulation measured by CD107a surface expression and Granzyme A secretion (Figures 2E and 2F, respectively).

These results suggest that CD8 T cells express functional PAR1, and its activation promotes an acceleration of calcium mobilization induced by TCR stimulation. In addition, PAR1 internalization maybe associated with factors stored in the cytotoxic granules that are released during granule exocytosis.

PAR1 inhibition impairs CD8 T cell cytotoxicity mediated by the granule exocytosis pathway

We next evaluated the potential role of PAR1 in CD8 T cell cytotoxic function mediated by the granule exocytosis pathway. To answer this question, we performed redirected killing assay using a FAS^{-} target L1210 (Catalfamo et al., 2004).

To determine GZB delivery we used an assay that measures its activity inside the target cells. The targets FAS^{-} L1210 were loaded with a quenched substrate that contained the GZB cleavage site, and upon delivery and processing by GZB, the substrate will lead to a fluorescent signal (Figure S2A). CellTrace Far Red (CTFR)-labeled FAS^{-}L1210 cells were incubated with activated human CD8 T cells at 27:1 effector to target (E:T) ratio in the presence or absence of an anti-human CD3 mAb and the GZB substrate. After one-hour incubation, cells were analyzed by flow cytometry. Target cells were gated on $CTFR^{+}$ cells, and GZB activity ($Substrate^{+}$) was analyzed (Figure 3A, gating strategy).

Activity of GZB was detected in the target cells only in presence of anti-CD3 mAb (Figures 3B and 3D). In addition, GZB delivery inside the target cells was efficiently blocked by a PAR1 antagonist SCH79797 in a concentration-dependent manner (Figures 3B and 3D).

In addition, we also determined the ability of CD8 T cells (Effectors, Figure 3A) to undergo degranulation by measuring the surface expression of CD107a (lysosomal-associated membrane protein 1, LAMP1) (Figure 3C) (Betts and Koup, 2004). In agreement with the inhibition of cytotoxicity observed in the presence of the PAR1 antagonist, surface expression of CD107a was reduced (Figures 3C and 3E). Accordantly, the inhibition of granule exocytosis by SCH79797 in CD8 T cells was also observed following measurements of the lysosome enzyme β-hexosaminidase and GZA in the supernatants of CD8 T cells following TCR stimulation (Figures S2B and S2C, respectively). Taken together, these results indicate that SCH79797 inhibition of PAR1 resulted in a significant impairment of the granule exocytosis pathway in CD8 T cells.

In contrast, the antagonist SCH530348 had no significant effect on GZB activity, and only a modest but significant reduction was noted on CD107a surface expression (Figure S2D). The reduced cytotoxicity was not due to increased cell death caused by the inhibitors (Figure S2E) but rather by differences in their effects of action. PAR1 inhibition by SCH79797 showed wider effects in CD8 T cell function including inhibition of IFNγ secretion and showed a trend in TNFα secretion although it did not reach statistical significance (Figure S2F). In contrast, SCH530348 inhibited TNFα secretion but not IFNγ (Figure S2F).

These results suggest that, in addition to cytokine secretion, PAR1 plays a role in CD8 T cell cytotoxicity mediated by the granule exocytosis pathway.

PAR1 inhibition leads to impaired granule exocytosis by reducing actin polymerization and altering microtubule-organizing center positioning at the immunological synapse

During the killing of target cells, the repositioning of the Microtubule Organizing Center (MTOC) toward the IS facilitates the polarized secretion of the cytolytic granules at secretory domain (Dieckmann et al., 2016; de Saint Basile et al., 2010; Dustin and Long, 2010; Jenkins and Griffiths, 2010; Stinchcombe and Griffiths, 2007; Stinchcombe et al., 2001, 2006; Tamzalit et al., 2019; Wurzer et al., 2019). PAR1 signaling through G12/13 mediates downstream cascade of events leading to cytoskeleton reorganization (Coughlin, 2001; Klages et al., 1999).

We then determined whether PAR1 inhibition impaired actin polymerization and/or repositioning of the MTOC toward the IS, interfering with the degranulation (Babich et al., 2012; de la Roche et al., 2013; Kumari et al., 2014; Tsun et al., 2011; Yu et al., 2013). CD8 T cells and FAS^{-}L1210 targets conjugates were prepared at 1:1 ratio and incubated for 20 min to allow the IS formation. Conjugates were examined for actin polymerization and MTOC movement by staining with phalloidin and alpha-tubulin, respectively. We evaluated the frequency of cells displaying the MTOC distal (Di), proximal (P), and docked (Do) at the IS as previously described (Lui-Roberts et al., 2012; Tsun et al., 2011). CD8 T-Target cell conjugates that were preincubated with the PAR1 antagonist SCH79797 showed a significant reduction in actin polymerization at the IS when compared with untreated controls (Figure 3F). In addition, PAR1 blockade inhibited the movement and repositioning of the MTOC at the IS. The majority of the conjugates displayed an MTOC either distal (40%) or proximal (50%) and only a 10% docked at the IS. In contrast, the large proportion of the conjugates incubated in media presented MTOCs that were proximal (43%) or docked (30%) at the IS (Figure 3G). These data suggest that PAR1 signaling is involved in repositioning of the MTOC, promoting the movement of the cytotoxic granules.

To confirm these observations, we evaluated the impact of PAR1 deficiency in murine lymphocytic choriomeningitis virus (LCMV) GP33-specific CD8 T cells (McGavern et al., 2002). LCMV TCR-Tg D^{b}GP33-41-specific CD8 T cells that are PAR1 deficient (referred as PAR1$^{-/-}$ P14 T cells) were generated by crossing the C57BL/6 D^{b}GP$_{33-41}$ TCR-tg P14 mice with the PAR1$^{-/-}$ mice. Wild-type (WT) or PAR1$^{-/-}$ P14 CD8 T cells were purified and activated *in vitro* with 1 μg/mL GP33 peptide for 2 days and expanded in the presence of interleukin-2 (IL-2) for an additional 3 to 5 days. *In vitro* activated WT or PAR1$^{-/-}$ P14 CD8 T cells were mixed at 1:1 ratio with GP33 peptide pulsed EL4 target cells and incubated for 20 min. Examination of the PAR1$^{-/-}$ P14-EL4 target conjugates showed similar effects to that observed of the PAR1 blockade in human CD8 T-Target cell conjugates. PAR1 deficiency in P14 CD8 T cells led to a reduced F-actin polymerization at the IS (Figure S3A). Evaluation of the MTOC repositioning showed that most of the conjugates had proximal MTOCs compared with the WT-EL4 conjugates (Figure S3B).

Accordant to this observation we found a reduced kinetic of CD107a surface expression in PAR1$^{-/-}$ P14 CD8 T cells compared with the WT P14 CD8 T cells (Figure S4A). Both WT and PAR1-deficient P14 T cells reached a plateau of maximum CD107a surface expression at a concentration of 10^{-4} μg/mL of LCMV GP33 peptide. In addition, the decreased ability of PAR1$^{-/-}$ P14 CD8 T cells to degranulate was associated with reduced killing of the GP33 peptide pulsed EL4 cells (substrate^{+} target cells) at low 3:1 E:T ratio. This effect was overcome at a higher E:T ratio (9:1) (Figure S4B). In addition, the reduced cytotoxic activity was not due to lower granzyme expression, because both WT and PAR1-deficient P14 T cells expressed comparable levels of both GZA and GZB (Figure S4C).

Altogether these data show that PAR1 signaling in CD8 T cells is involved in actin polymerization and repositioning of the MTOC, facilitating the movement of cytotoxic granules toward the IS.

PAR1$^{-/-}$ CD8 T cells display decreased cytokine secretion and reduced viral clearance during LCMV infection

To investigate the role of PAR1 in CD8 T cell function *in vivo*, we performed infection with LCMV using PAR1-deficient mice (Connolly et al., 1996). The naive PAR1$^{-/-}$ global knockout mice had no apparent phenotype. Examination of the lymph organs showed similar cell counts in the lymph nodes as WT animals, and PAR1$^{-/-}$ mice displayed a lower trend of cell number in the spleens (Figures S5A and S5B). Similar cell numbers and frequencies of eosinophils, neutrophils, monocytes, and conventional and plasmacytoid dendritic cells were observed in both spleens and lymph nodes of PAR1$^{-/-}$ and WT mice (Figure S5C). In addition, no significant differences were observed in the cell counts and frequencies of lymphocytes subsets including T, B, and natural killer (NK) cells (Figures S6A and S6B). Furthermore, both WT and PAR1-deficient CD4 and CD8 T cells had similar phenotype (naive, Central Memory, and Effector memory) and proliferative capacity upon *in vitro* TCR stimulation (Figures S6C and S6D).

To elucidate the role of PAR1 receptor *in vivo*, we used the murine LCMV system, which is a well-characterized murine model to the study of the dynamics of CD8 T-cell-mediated immunity during a viral infection (Buchmeier et al., 1980; van der Most et al., 1998; Wherry et al., 2003; Zinkernagel et al., 1986). We challenged the mice with LCMV WE 2.5, a virus strain with tropism for the liver, to evaluate trafficking properties of the virus-specific T cells (Cerny et al., 1988). At day 8 postinfection (p.i), similar frequencies and counts of

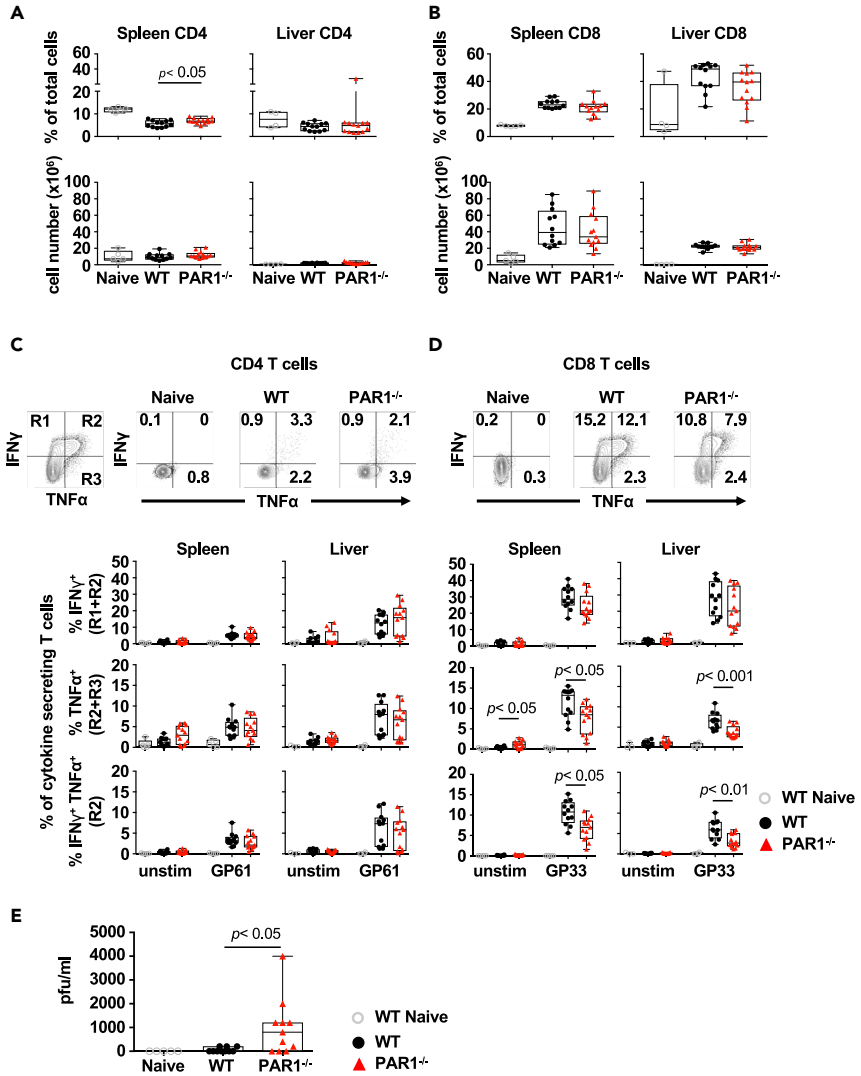

Figure 4. Delayed viral clearance and decreased cytokine secretion by PAR1$^{-/-}$ CD8 T cells

(A and B) PAR1$^{-/-}$ and WT littermates were intravenously infected with 2 × 10^5 pfu of LCMV WE 2.5 strain. At day 8 postinfection, frequency and counts of cells in the spleen and liver were analyzed: (A) CD4 T cells, (B) CD8 T cells.

(C) Isolated spleen and liver cells from infected mice (n = 13) and uninfected naive control were stimulated *in vitro* with LCMV GP61 peptides. Percentage of CD4 T cells secreting cytokines IFNγ and TNFα.

(D) Isolated splenic and liver CD8 T cells from infected mice (n = 13) and uninfected naive control were stimulated *in vitro* with LCMV GP33 peptides for 5 h. Percentage of CD8 T cells secreting IFNγ and TNFα.

(E) Viral titer was determined by plaque assay in collected serum samples (n = 11). Data are presented as box and whisker plot of median value with interquartile range from all animals pooled from three independent experiments. Statistical analysis was performed using nonparametric Mann-Whitney test. *p* value <0.05 was considered significant.

bulk CD4 and CD8 T cells were observed in the spleen and liver of WT and PAR1$^{-/-}$ mice (Figures 4A and 4B). In addition, we assessed the ability of LCMV-specific CD4 and CD8 T cells to secrete cytokines in response to *in vitro* stimulation with LCMV MHC class II restricted epitope (GP61) and class I restricted immunodominant (GP33, NP396) and subdominant (GP276, NP205) epitopes (Figures 4C, 4D, and S7). No significant changes in GP61-specific CD4 T cells were observed (Figure 4C). In contrast, PAR1-deficient CD8 T cells had a reduced frequency of TNFα$^+$ and IFNγ$^+$ TNFα$^+$ GP33-specific CD8 T cells in both spleen and liver (Figure 4D). The reduced functional capacity of CD8 T cells was associated with an elevated viral load in the serum of PAR1-deficient mice at day 8 p.i (Figure 4E). These data suggest that PAR1 plays a role in CD8 T cell function during LCMV viral infection.

PAR1-deficient P14 T cells showed a reduced expansion and cytokine secretion

We next evaluated the mechanisms in which PAR1 signaling alters the ability of CD8 T cells to eliminate the virus in the context of LCMV infection. Because PAR1 is expressed by multiple cells, we performed adoptive cell transfer experiments of purified naive CD45.2$^+$ WT and PAR1$^{-/-}$ P14 CD8 T cells into congenic CD45.1$^+$ B6 recipient mice, to evaluate the impact of PAR1 deficiency in virus-specific CD8 T cells.

We determined the *in vivo* expansion capacity of WT and PAR1$^{-/-}$ P14 T cells in the spleen and liver at day 6 p.i. The frequency of splenic and liver PAR1$^{-/-}$ P14 CD8 T cells was significantly reduced compared with the WT P14 CD8 T cells (Figure 5A). In addition, the total PAR1$^{-/-}$ P14 T cell numbers were reduced only in the liver, suggesting a potential trafficking delay of the PAR1-deficient P14 CD8 T cells (Figure 5A). In addition, in the liver, the frequency of PAR1$^{-/-}$ P14 CD8 T cells producing IFNγ^+ was significantly reduced compared with the WT, and this effect was not observed in the spleen (Figure 5B). The cell numbers of IFNγ^+, TNFα^+, and IFNγ^+TNFα^+ PAR1-deficient P14 CD8 T cells was also markedly decreased in the liver compared with the WT P14 CD8 T cells (Figure S8A). The PAR1-deficient P14 CD8 T cells showed no differences to the WT cells in terms of differentiation (CD8 T central and effector memory) and the expression of chemokine receptors CXCR3 and CX3CR1 involved in the recruitment of T cells into peripheral tissues (Figure S8B).

To better evaluate the expansion and migration properties of the PAR1-deficient CD8 T cells in a competitive environment, we performed an adoptive cell transfer experiment of WT and PAR1$^{-/-}$ P14 CD8 T cells into the same host (Figure S9). In this adoptive cell transfer condition, the frequency and cell numbers of the PAR1$^{-/-}$ P14 CD8 T cells were reduced in the spleen and the liver compared with the WT P14 CD8 T cells (Figure S9B). PAR1$^{-/-}$ P14 CD8 T cells showed an increased frequency of effector phenotype defined by surface expression of KLRG1^{high}CD127^{low} (Figure S9C) (Joshi et al., 2007). Despite the more differentiated phenotype, the frequency of PAR1$^{-/-}$ P14 CD8 T cells secreting IFNγ was reduced in the liver (Figure S9D). In addition, the cell numbers of PAR1$^{-/-}$ P14 CD8 T cells secreting cytokines (IFNγ^+, TNFα^+, and IFNγ^+TNFα^+) were significantly reduced in the liver (Figure S9D).

These data suggest that PAR1-deficient LCMV-GP33-specific CD8 T cells do not expand efficiently in the spleen, and there is reduced recruitment/function of these cells in the liver after infection. In addition, in a competitive environment PAR1-deficient LCMV-GP33-specific CD8 T cells showed increase in short-lived effector phenotype, suggesting differences in the expansion and/or survival compared with the WT counterparts.

To next determine the heterogeneity, potential trafficking, and functional differences between WT and PAR1$^{-/-}$ effector P14 T cells, we evaluated the expression of IFNγ, TNFα, CD107a, CXCR3, CX3CR1, and CD27 using flow self-organizing map (FlowSOM). The FlowSOM algorithm allows to generate an automated distribution and visualization of highly similar cells by analyzing expression of a group of selected markers (Van Gassen et al., 2015). FlowSOM maps (selected eight number of clusters for the analysis) were generated by concatenating 10^5 of total CD8 T cells (recipient and donor P14 CD8 T cells) from the spleens and livers of the LCMV-infected mice at day 6 p.i.

The expression of markers associated with trafficking and function of CD8 T cells is shown in the pie. To identify the donor P14 T cells we used expression of CD45.2 (Figure 6A). The clusters contained a series of nodes with heterogeneous CD8 T cell populations (both recipient and donor P14 CD8 T cells). The relative abundance of each node within a cluster is proportional to the size of the black circle inside the node displayed in the figure. We found that CD45.2$^+$ P14 CD8 T cells (bright green inside the pie) resided mostly in clusters 5 and 7, and a very discreet cluster 6 (purple) was also observed (Figure 6A). Cluster 5 (blue color) contained most of the P14 T cells with low to intermediate expression of CD107a (brown wedge inside pie chart) and low levels of cytokines IFNγ (light blue wedge) and TNFα (dark blue wedge). In contrast, P14 T cells expressing higher levels of TNFα and IFNγ, as well as high levels of CD107a were enriched in cluster 7 (pink color, Figure 6A).

These data show a heterogeneity of effector P14 CD8 T cells (WT and PAR1$^{-/-}$) with cells that have the capacity to degranulate and secrete cytokines (cluster 7). In contrast, cluster 5 was enriched in cells that expressed lower levels of cytokines and have cytotoxic potential measured by CD107a. Similar heterogeneity was observed when only P14 CD8 T cells were concatenated and analyzed in FlowSOM (Figure S10).

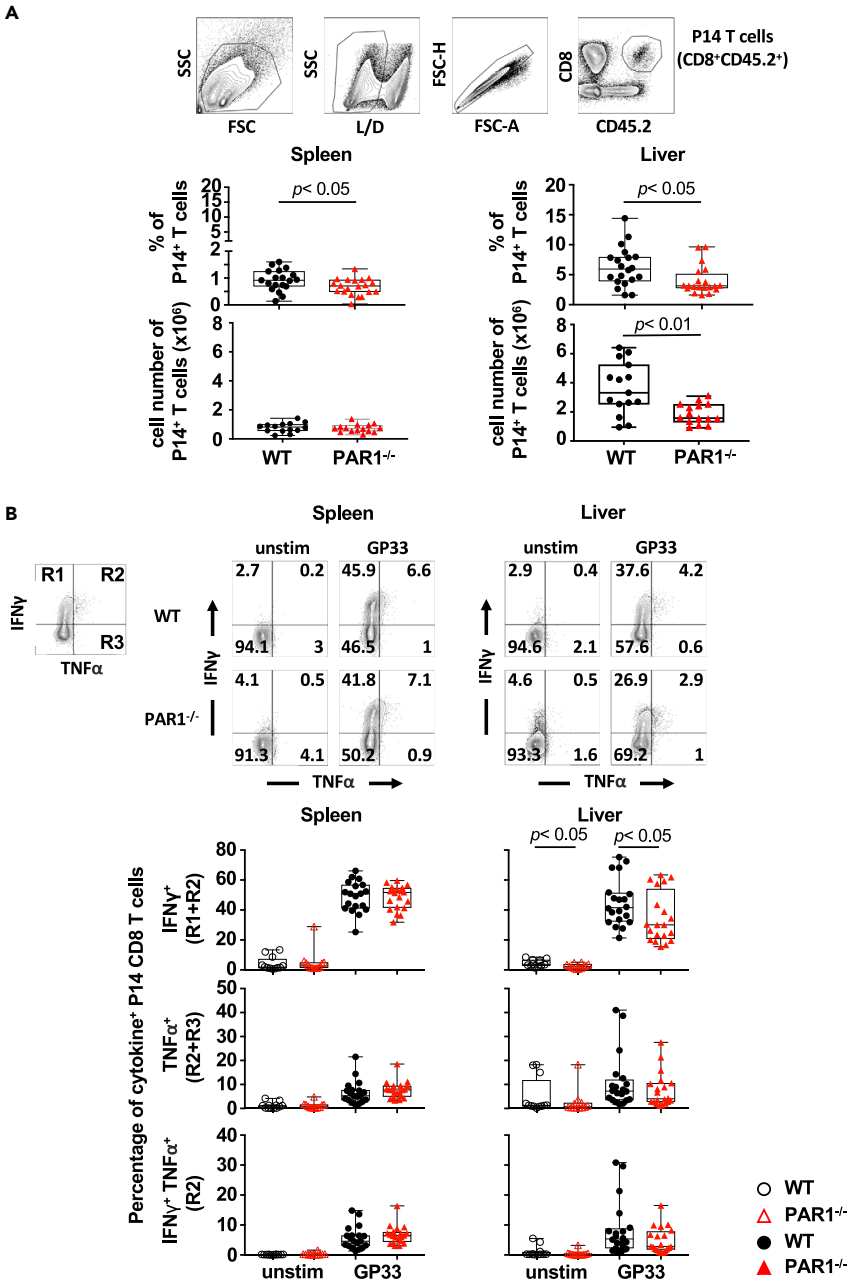

Figure 5. Reduced expansion and function of adoptively transferred PAR1$^{-/-}$ P14 T cells during LCMV infection

P14 CD8 T cells (10^4 T cells) purified from lymph node of WT and PAR1$^{-/-}$ mice (B6.P14.CD45.2.Thy1.1) were adoptively transferred (i.v.) into CD45.1.Thy1.2 recipient mice, respectively. Recipient mice were infected the next day with LCMV WE 2.5 strain (2×10^5 pfu, i.v). Six days postinfection, splenic and liver cells were isolated and *in vitro* stimulated with LCMV GP33 peptides for 4 h. Cells were stained for markers listed in Table 3. (A) Gating strategy to analyze adoptively transferred P14 T cells. Percentage and cell numbers of P14 CD8 T cells in the spleen and liver are expressed as frequency of total live cells.

(B) Gating strategy for the analysis of the P14 CD8 T cells in the spleen and liver that are IFNγ$^+$ (R1+R2), TNFα$^+$ (R2+R3), or IFNγ$^+$TNFα$^+$ (R2). The graph is presented as box and whisker plot and shows the median value with interquartile range, from all animals pooled from four independent experiments (n = 20). Statistical analysis was performed using nonparametric Mann-Whitney test. *p* value <0.05 was considered significant.

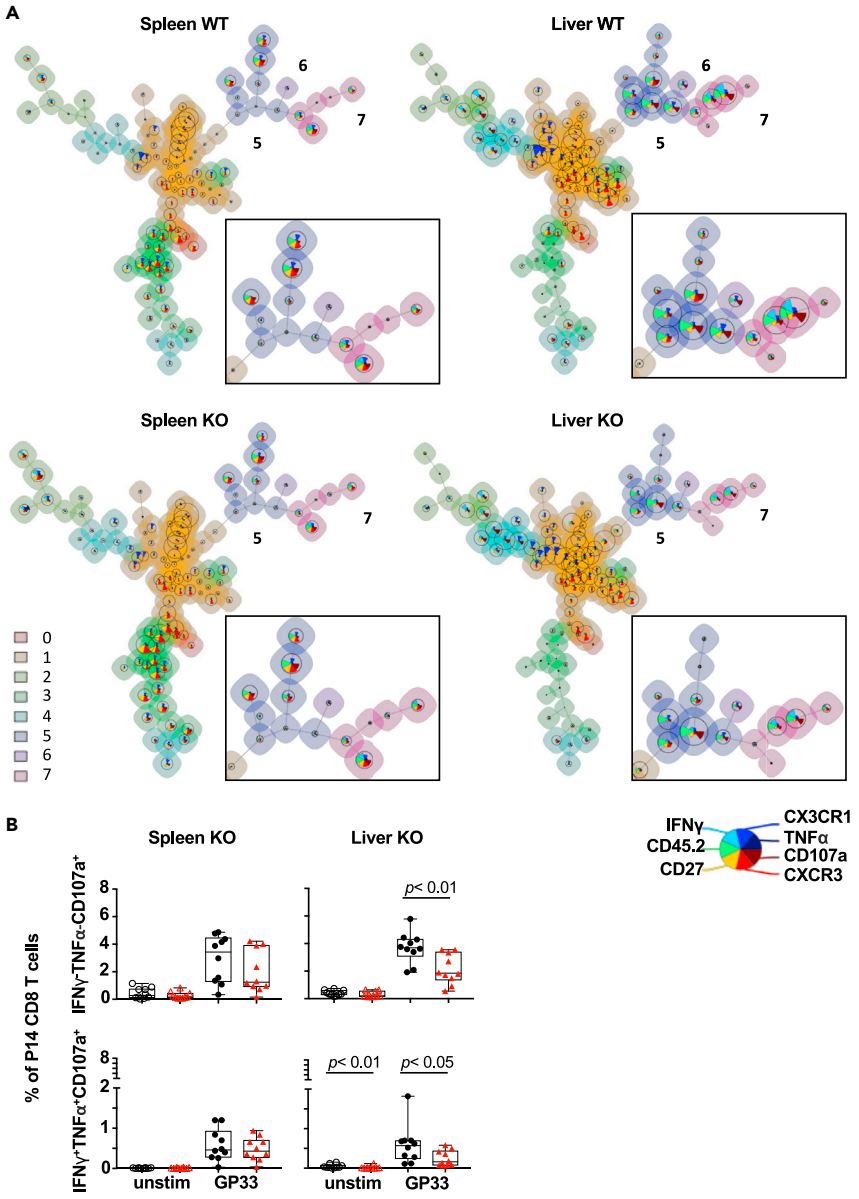

Figure 6. Heterogeneous populations of PAR1$^{-/-}$ P14 T cells during P14 adoptive transfer

Multidimensional single-cell analysis was performed using FlowSOM algorithm. To allow comparisons between the groups, a FlowSOM map was generated with concatenating 10^5 total CD8 T cells (recipient and WT and PAR1$^{-/-}$ P14 CD8 T cells) from spleen and liver. The FlowSOM map (selected 8 clusters for analysis) was then applied to each condition for the clustering of CD8 T cells. Maps were generated by selecting the following markers: IFNγ, TNFα, CD107a, CXCR3, CX3CR1, CD27, and CD45.2 noted with wedge color inside the pie chart. Eight clusters were generated, and cluster 5, 6, and 7 that contain CD45.2$^+$ P14 CD8 T cells are magnified for visualization in the lower right panel of each condition. (A) Representative maps were shown from one of three independent experiments.

(B) Standard manual gating analysis of the adoptively transferred CD45.2$^+$ P14 CD8 T cells that express IFNγ$^+$TNFα$^+$CD107a$^+$ and IFNγ$^-$TNFα$^-$CD107a$^+$, corresponding to the cluster 5 and 7 in FlowSOM. Percentage was expressed as frequency of total CD8 T cells. The box and whisker plot showed median value with interquartile range. Data were pooled from two independent experiments (n = 10). Statistical analysis was performed using nonparametric Mann-Whitney test.

These results were further confirmed using conventional gating analysis (Figure 6B). We found a reduced frequency of PAR1$^{-/-}$ P14 CD8 T cells that were IFNγ$^+$TNFα$^+$CD107a$^+$ and IFNγ$^-$TNFα$^-$CD107a$^+$ in the liver (Figure 6B). No changes in the expression of chemokine receptors CXCR3, CX3CR1, and CXCR4

and differentiation markers CD27, CD127, KLRG1, CD44, CD62L, and CD69 were observed between WT and PAR1-deficient P14 T cells (Figure S8). These results indicate that effector P14 T cells constitute a heterogeneous population, which in the case of PAR1$^{-/-}$ P14 T cells, appear to have a diminished potential for executing effector functions.

DISCUSSION

In this study we investigated the underlying mechanisms of PAR1-mediated modulation of CD8 T cell cytotoxic function. In human CD8 T cells, PAR1 expression was associated with memory and effector differentiation. In addition, PAR1 signaling was involved in F-actin accumulation and MTOC repositioning toward the immunological synapse, two important processes that facilitated the polarized secretion of effector molecules during cytotoxicity (Dustin and Long, 2010; Jenkins and Griffiths, 2010; Migueles et al., 2008; Stinchcombe and Griffiths, 2007). *In vivo*, during LCMV infection, PAR1-deficient P14 T cells showed a decreased expansion and/or trafficking to peripheral tissues and reduced antiviral cytokine production. These data indicate that PAR1 plays a role in CD8 T cell function.

PAR1 activation by thrombin in platelets has been shown to signal through Gq and G12/13, connecting PLCβ and Rho-mediated ROCK pathways, respectively (Coughlin, 2000; Hung et al., 1992; Jin et al., 2009; Klages et al., 1999; Ramachandran et al., 2012; Soh et al., 2010). Previous studies have shown that TCR stimulation can activate G proteins; however, the receptor connecting these two signaling pathways has not been defined (Bueno et al., 2006; Ngai et al., 2008; Stanners et al., 1995). In the present study, we found that in absence of thrombin surface PAR1 expression was reduced upon TCR stimulation. PAR1 blockade in human CD8 T cells attenuated TCR-induced calcium mobilization, suggesting a potential crosstalk between PAR1 and TCR signaling pathways. Supporting these observations, previous reports demonstrated that activation of PAR1 induced tyrosine phosphorylation of the TCR signaling cascade including ZAP70 and SLP76, as well as vav1, a Rho-family guanine exchange factor that activates Rho GTPases, regulating cytoskeleton reorganization (Bar-Shavit et al., 2002). Downstream these early TCR signaling events, activation of PAR1 by thrombin enhanced TCR-induced IFNγ secretion by human CD8 T cells (Hurley et al., 2013).

PAR1 signaling through G12/13 induces Rho-mediated ROCK pathways, leading to cytoskeletal changes and the clustering of F-actin and CD3 molecules in membrane domain (Fujimoto et al., 2013; Hatziapostolou et al., 2008; Hurley et al., 2013; Otani et al., 2011; Sharma et al., 2017; Vouret-Craviari et al., 1998; Yin et al., 2003). F-actin polymerization is important in proximal TCR signaling and regulates T cell activation (Babich et al., 2012; Campi et al., 2005; Kumari et al., 2014; Varma et al., 2006; Yu et al., 2013). Importantly, our data show that disruption of PAR1 signaling on CD8 T cells influences the movement of the MTOC, an important event that facilitate the polarized secretion of cytotoxic granules content at IS (de Saint Basile et al., 2010; Henkart, 1994). These effects were reflected in the reduced ability of the CD8 T cells to kill target cells *in vitro*.

In addition to thrombin, PAR1 can be activated by other serine proteases stored in the cytotoxic granules such as granzymes (Cooper et al., 2011; Lee et al., 2017; Suidan et al., 1994; Wang et al., 2012). Granzyme A and B have been reported to be responsible for PAR1 activation in neurons, and it can induce neurotoxicity *in vitro* (Lee et al., 2017; Wang et al., 2012). Specifically, T lymphocytes released GZA and mediated cellular responses of neurons and astrocytes through the activation of PAR1. We showed that TCR activation induced loss of surface PAR1 staining, and this occurs concomitant with the granule content release measured by surface expression of lysosome membrane protein CD107a and detection of GZA and β-hexosaminidase in the supernatants (Figures 2C, 2E and 2F, S2B, and S2C). Whether granzymes can directly activate PAR1 in the CD8 T cells and participate in a feedback loop during granule exocytosis requires further investigation.

We previously showed that PAR1 activation by thrombin increases IFNγ secretion (Hurley et al., 2013). In the present study, we observed distinct inhibitory effects in CD8 T cells by two PAR1 antagonists (SCH79797 and SCH530348). SCH530348 blocked TCR-induced calcium mobilization, an early event in the TCR signaling cascade that led to reduced TFNα secretion by CD8 T cells. In contrast, SCH79797 had a wider effect reducing cytotoxicity and cytokine secretion. The SCH79797 inhibitor has been reported to have off-target effects and inhibits cell proliferation and induces apoptosis in a PAR1-independent fashion (Di Serio et al., 2007; Gupta et al., 2018). In our present and previous reports, we have limited exposure to

SCH79797 in the vitro experiments monitoring viability and motility in response to sequential activation with thrombin and chemokines in the same cells (Hurley et al., 2013). We reported that blockade of PAR1 signaling inhibited chemokinesis and reorganization of the cytoskeleton induced by thrombin stimulation without affecting the response of the same T cells to a chemokine stimulus. Conversely, the blockade of the Gi protein (coupled to chemokine receptors) with pertussis toxin, it did not alter the motility and cytoskeleton reorganization in response to thrombin, suggesting a specific effect of this inhibitor (Hurley et al., 2013). These observations suggest that SCH79797 inhibit PAR1 signaling. In addition, the effects observed in the human CD8 T cells mimicked those observed in PAR1-deficient murine CD8 T cells during antigen recognition, suggesting that SCH79797 on CD8 T cells is mediated by PAR1 inhibition. However, we cannot exclude other off-target effects of this inhibitor. In addition, the PLC inhibitor blocked TCR-induced calcium mobilization; however, no effect was observed when T cells were stimulated with thrombin. The differences in the concentration of the PLC inhibitor could be a contributor factor to the lack of inhibition when compared with the inhibitory effects observed in thrombin-induced calcium mobilization on human platelets (Heemskerk et al., 1997). The efficient inhibition on calcium mobilization by SCH79797 and SCH530348 suggest that thrombin activated PLC in human CD8 T cells.

In the context of viral infections, PAR1 was shown to be involved in the innate responses; however, its role in T cell function was not well defined (Antoniak et al., 2013; Khoufache et al., 2013; Le et al., 2018; Scholz et al., 2004; Sutherland et al., 2007). The naive PAR1$^{-/-}$ global knockout mice had no apparent phenotype in terms of frequencies and number of cells. We used the LCMV model of infection in which CD8 T cells play a major role in viral control/elimination. In addition, the infection with the LCMV WE strain that has liver tropism allowed us to evaluate the trafficking of virus-specific CD8 T cells (Leist et al., 1989; Oehen et al., 1991; Zinkernagel et al., 1986). The *in vivo* effects of PAR1 deficiency in polyclonal-virus-specific T cells in the global PAR1 knockout mice led to a failure of efficiently control LCMV infection. The delay in the viral clearance was heterogeneous among the animals as shown in the viral titers in the plasma, and it was associated with lower frequencies and a reduced ability to secrete cytokines by virus-specific CD8 T cells in the liver. This effect was mostly observed in CD8 T cells specific to the immunodominant epitope LCMV-GP33 and in less degree to the subdominant epitopes (Figure S7) (Gairin et al., 1995; Klenerman and Zinkernagel, 1998; van der Most et al., 1998). The effect of PAR1 deficiency was more apparent in the liver than the spleen and may reflect a delay in the trafficking properties of virus-specific CD8 T cells into the tissue. Whether these effects are accompanied with more tissue viral titers and tissue pathology needs further investigation.

In addition, in the global PAR1$^{-/-}$ mice, the deficiency of PAR1 signaling in innate cells will impact the activation and differentiation of virus-specific CD8 T cells. Studies in a mouse model of severe lipopolysaccharide (LPS) challenge showed that PAR1 signaling is involved in the recruitment of dendritic cells, promoting disseminated intravascular coagulation (Niessen et al., 2008). Moreover, in a viral infection model of coxsackievirus-B3-induced (CVB3-induced) myocarditis infection, PAR1 signaling enhanced IFN-β and CXCL10 expression in cardiac fibroblasts and promoted activation of innate responses. Similar observations were reported during influenza infection (Antoniak et al., 2013, 2017, 2021). Modulating PAR1 signaling by antagonists or agonists was tested *in vivo* and demonstrates the role of PAR1 in the setting of viral infections (Aerts et al., 2013; Khoufache et al., 2013; Le et al., 2018). Although in these studies T cell function has not been directly addressed, one could predict that alteration of the innate responses will impact T-cell-mediated immunity. In addition, platelets also participate in immunity against pathogens and can regulate T cell function (Green et al., 2015; Lam et al., 2015; Mudd et al., 2016). In the PAR1$^{-/-}$ mice, the contribution of platelets in modulating T cell responses should be preserved because mouse platelets do not express PAR1 (PAR4 and PAR3 are the receptors for thrombin) (Connolly et al., 1996; Ishihara et al., 1998; Kahn et al., 1998, 1999; Xu et al., 1998). Future studies should address the potential interaction of virus-specific T cells and platelets in regulating T cell function at different stages of the infection.

To evaluate the effect of PAR1 signaling only in CD8 T cells our adoptive transfer studies with WT and PAR1$^{-/-}$ P14 CD8 T cells revealed that PAR1 deficiency led to a decreased effector CD8 T cells in the liver with reduced capacity to produce antiviral cytokines. In addition, when both PAR1$^{-/-}$ and WT P14 T cells were transferred into the same host, a decreased frequency of PAR1$^{-/-}$ P14 CD8 T cells was observed in both spleen and liver. In this condition, PAR1-deficient P14 CD8 T cells showed an increase in short-lived effector phenotype (CD127^{low}KLRG1^{high}) compared with the WT counterpart, indicating a potential disadvantage in the expansion and/or survival. Compared with the WT P14 CD8 T cells, PAR1$^{-/-}$ CD8 T cells showed reduced frequencies of the memory precursors (CD127^{high}KLRG1^{low}). Previous studies had shown

that between 5 and 8 days p.i, CD8 T cells gain expression of CD127 and differentiate into two distinct cell lineages CD127^{low}KLRG1^{high} and memory precursors CD127^{high}KLRG1^{low} (Joshi et al., 2007). Whether PAR1 signaling alters the development of memory precursors warrants further investigation.

Altogether this study highlights the important role of PAR1 in CD8 T cell function. PAR1 signaling can potentially be modulated in scenarios required to reduce CD8 T-cell-mediated immunopathology or to increase cytotoxic function such as chronic infections. In the future, to further address the contribution of PAR1, PAR1 flox mice will be used to investigate the role of PAR1 in specific cell types.

Limitations of study

In the present study, we performed a comprehensive study about the role of PAR1 in CD8 T cell function with a focus on CD8 T cell cytotoxicity. In human CD8 T cells the pharmacological inhibition of PAR1 signaling recapitulated the same defects observed in CD8 T cells from a PAR1-deficient mice in the formation of the immunological synapse and the polarized secretion of cytotoxic granules. We found differences in the mode of action of this inhibitor, suggesting that may block specific pathway and/or have other off-target effects. These suggest that PAR1 signaling may regulate distinct signaling pathways in CD8 T cell function.

In the adoptive T cell transfer experiments in the setting of LCMV infection, we found that PAR1 deficiency was rather mild, and future experiments should address the impact of PAR1 signaling in immunity against viruses using conditional knock-out mice to evaluate its contribution in other cells during infection.

STAR★METHODS

Detailed methods are provided in the online version of this paper and include the following:

- KEY RESOURCES TABLE
- RESOURCE AVAILABILITY
  - Lead contact
  - Materials availability
  - Data and code availability
- EXPERIMENTAL MODEL AND SUBJECT DETAILS
  - Human CD8 T cell isolation and culture
  - Mice
- EXPERIMENTAL MODEL AND SUBJECT DETAILS
  - Methods details
- QUANTIFICATION AND STATISTICAL ANALYSIS

SUPPLEMENTAL INFORMATION

Supplemental information can be found online at https://doi.org/10.1016/j.isci.2021.103387.

ACKNOWLEDGMENTS

Research reported in this publication was supported by the National Institute of Allergy and Infectious Diseases of the National Institutes of Health under award number NIH R01AI145549-02 as well as the National Institute of Neurological Disorders and Stroke intramural program (DBM and JH). MC is supported in part by Leidos Biomedical Research, Inc. and has been funded in whole or in part with federal funds from the National Cancer Institute, NIH, under Contract HHSN261200800001E. The content of this publication does not necessarily reflect the views or policies of the Department of Health and Human Services, nor does mention of trade names, commercial products, or organizations imply endorsement by the US Government.

AUTHOR CONTRIBUTIONS

MC conceived the study; PMI, DBM, and MC designed the experiments. HC, MS, TL, RH, AG, and JAM performed human CD8 T cell experiments. HC, JH, CL, TL, ZZ, and JC performed mouse experiments. TK guided microscopy acquisition and data analysis. HC, MS, and MC wrote the paper. JAM, PMI, and DBM critically reviewed the manuscript.

DECLARATION OF INTERESTS

The authors have no conflict of interest to declare.

Received: April 9, 2021
Revised: September 28, 2021
Accepted: October 28, 2021
Published: November 19, 2021

REFERENCES

Aerts, L., Hamelin, M.E., Rheaume, C., Lavigne, S., Couture, C., Kim, W., Susan-Resiga, D., Prat, A., Seidah, N.G., Vergnolle, N., et al. (2013). Modulation of protease activated receptor 1 influences human metapneumovirus disease severity in a mouse model. PLoS One *8*, e72529.

Ahn, H.S., Foster, C., Boykow, G., Stamford, A., Manna, M., and Graziano, M. (2000). Inhibition of cellular action of thrombin by N3-cyclopropyl-7-[[4-(1-methylethyl)phenyl]methyl]-7H-pyrrolo[3, 2-f]quinazoline-1,3-diamine (SCH 79797), a nonpeptide thrombin receptor antagonist. Biochem. Pharmacol. *60*, 1425–1434.

Antoniak, S., Owens, A.P., Baunacke, M., Williams, J.C., Lee, R.D., Weithauser, A., Sheridan, P.A., Malz, R., Luyendyk, J.P., Esserman, D.A., et al. (2013). PAR-1 contributes to the innate immune response during viral infection. J. Clin. Invest. *123*, 1310–1322.

Antoniak, S., Tatsumi, K., Bode, M., Vanja, S., Williams, J.C., and Mackman, N. (2017). Protease-activated receptor 1 enhances poly I:C induction of the antiviral response in Macrophages and mice. J. Innate Immun. *9*, 181–192.

Antoniak, S., Tatsumi, K., Schmedes, C.M., Egnatz, G.J., Auriemma, A.C., Bharathi, V., Stokol, T., Beck, M.A., Griffin, J.H., Palumbo, J.S., and Mackman, N. (2021). PAR1 regulation of CXCL1 expression and neutrophil recruitment to the lung in mice infected with influenza A virus. J. Thromb. Haemost. *19*, 1103–1111.

Arora, P., Ricks, T.K., and Trejo, J. (2007). Protease-activated receptor signalling, endocytic sorting and dysregulation in cancer. J. Cell Sci. *120*, 921–928.

Babich, A., Li, S., O'connor, R.S., Milone, M.C., Freedman, B.D., and Burkhardt, J.K. (2012). F-actin polymerization and retrograde flow drive sustained PLCgamma1 signaling during T cell activation. J. Cell Biol. *197*, 775–787.

Bar-Shavit, R., Maoz, M., Yongjun, Y., Groysman, M., Dekel, I., and Katzav, S. (2002). Signalling pathways induced by protease-activated receptors and integrins in T cells. Immunology *105*, 35–46.

Betts, M.R., and Koup, R.A. (2004). Detection of T-cell degranulation: CD107a and b. Methods Cell Biol. *75*, 497–512.

Billadeau, D.D., Nolz, J.C., and Gomez, T.S. (2007). Regulation of T-cell activation by the cytoskeleton. Nat. Rev. Immunol. *7*, 131–143.

Buchmeier, M.J., Welsh, R.M., Dutko, F.J., and Oldstone, M.B. (1980). The virology and immunobiology of lymphocytic choriomeningitis virus infection. Adv. Immunol. *30*, 275–331.

Bueno, C., Lemke, C.D., Criado, G., Baroja, M.L., Ferguson, S.S., Rahman, A.K., Tsoukas, C.D., Mccormick, J.K., and Madrenas, J. (2006). Bacterial superantigens bypass Lck-dependent T cell receptor signaling by activating a Galpha11-dependent, PLC-beta-mediated pathway. Immunity *25*, 67–78.

Buggert, M., Tauriainen, J., Yamamoto, T., Frederiksen, J., Ivarsson, M.A., Michaelsson, J., Lund, O., Hejdeman, B., Jansson, M., Sonnerborg, A., et al. (2014). T-bet and Eomes are differentially linked to the exhausted phenotype of CD8+ T cells in HIV infection. PLoS Pathog. *10*, e1004251.

Campi, G., Varma, R., and Dustin, M.L. (2005). Actin and agonist MHC-peptide complex-dependent T cell receptor microclusters as scaffolds for signaling. J. Exp. Med. *202*, 1031–1036.

Catalfamo, M., and Henkart, P.A. (2003). Perforin and the granule exocytosis cytotoxicity pathway. Curr. Opin. Immunol. *15*, 522–527.

Catalfamo, M., Karpova, T., Mcnally, J., Costes, S.V., Lockett, S.J., Bos, E., Peters, P.J., and Henkart, P.A. (2004). Human CD8+ T cells store RANTES in a unique secretory compartment and release it rapidly after TcR stimulation. Immunity *20*, 219–230.

Cerny, A., Sutter, S., Bazin, H., Hengartner, H., and Zinkernagel, R.M. (1988). Clearance of lymphocytic choriomeningitis virus in antibody- and B-cell-deprived mice. J. Virol. *62*, 1803–1807.

Chen, D., and Dorling, A. (2009). Critical roles for thrombin in acute and chronic inflammation. J. Thromb. Haemost. *7*, 122–126.

Connolly, A.J., Ishihara, H., Kahn, M.L., Farese, R.V., JR., and Coughlin, S.R. (1996). Role of the thrombin receptor in development and evidence for a second receptor. Nature *381*, 516–519.

Cooper, D.M., Pechkovsky, D.V., Hackett, T.L., Knight, D.A., and Granville, D.J. (2011). Granzyme K activates protease-activated receptor-1. PLoS One *6*, e21484.

Coughlin, S.R. (2000). Thrombin signalling and protease-activated receptors. Nature *407*, 258–264.

Coughlin, S.R. (2001). Protease-activated receptors in vascular biology. Thromb. Haemost. *86*, 298–307.

Cunningham, M.A., Rondeau, E., Chen, X., Coughlin, S.R., Holdsworth, S.R., and Tipping, P.G. (2000). Protease-activated receptor 1 mediates thrombin-dependent, cell-mediated renal inflammation in crescentic glomerulonephritis. J. Exp. Med. *191*, 455–462.

de la Roche, M., Ritter, A.T., Angus, K.L., Dinsmore, C., Earnshaw, C.H., Reiter, J.F., and Griffiths, G.M. (2013). Hedgehog signaling controls T cell killing at the immunological synapse. Science *342*, 1247–1250.

de Saint Basile, G., Menasche, G., and Fischer, A. (2010). Molecular mechanisms of biogenesis and exocytosis of cytotoxic granules. Nat. Rev. Immunol. *10*, 568–579.

Di Serio, C., Pellerito, S., Duarte, M., Massi, D., Naldini, A., Cirino, G., Prudovsky, I., Santucci, M., Geppetti, P., Marchionni, N., et al. (2007). Protease-activated receptor 1-selective antagonist SCH79797 inhibits cell proliferation and induces apoptosis by a protease-activated receptor 1-independent mechanism. Basic Clin. Pharmacol. Toxicol. *101*, 63–69.

Dieckmann, N.M., Frazer, G.L., Asano, Y., Stinchcombe, J.C., and Griffiths, G.M. (2016). The cytotoxic T lymphocyte immune synapse at a glance. J. Cell Sci. *129*, 2881–2886.

Dustin, M.L., and Long, E.O. (2010). Cytotoxic immunological synapses. Immunol. Rev. *235*, 24–34.

Fujimoto, D., Hirono, Y., Goi, T., Katayama, K., Matsukawa, S., and Yamaguchi, A. (2013). The activation of proteinase-activated receptor-1 (PAR1) promotes gastric cancer cell alteration of cellular morphology related to cell motility and invasion. Int. J. Oncol. *42*, 565–573.

Gairin, J.E., Mazarguil, H., Hudrisier, D., and Oldstone, M.B. (1995). Optimal lymphocytic choriomeningitis virus sequences restricted by H-2Db major histocompatibility complex class I molecules and presented to cytotoxic T lymphocytes. J. Virol. *69*, 2297–2305.

Gaud, G., Lesourne, R., and Love, P.E. (2018). Regulatory mechanisms in T cell receptor signalling. Nat. Rev. Immunol. *18*, 485–497.

Geiger, B., Rosen, D., and Berke, G. (1982). Spatial relationships of microtubule-organizing centers and the contact area of cytotoxic T lymphocytes and target cells. J. Cell Biol. *95*, 137–143.

Grakoui, A., Bromley, S.K., Sumen, C., Davis, M.M., Shaw, A.S., Allen, P.M., and Dustin, M.L. (1999). The immunological synapse: a molecular machine controlling T cell activation. Science *285*, 221–227.

Green, S.A., Smith, M., Hasley, R.B., Stephany, D., Harned, A., Nagashima, K., Abdullah, S., Pittaluga, S., Imamichi, T., Qin, J., et al. (2015).

Activated platelet-T-cell conjugates in peripheral blood of patients with HIV infection: coupling coagulation/inflammation and T cells. AIDS *29*, 1297–1308.

Gupta, N., Liu, R., Shin, S., Sinha, R., Pogliano, J., Pogliano, K., Griffin, J.H., Nizet, V., and Corriden, R. (2018). SCH79797 improves outcomes in experimental bacterial pneumonia by boosting neutrophil killing and direct antibiotic activity. J. Antimicrob. Chemother. *73*, 1586–1594.

Harnett, M., and Rigley, K. (1992). The role of G-proteins versus protein tyrosine kinases in the regulation of lymphocyte activation. Immunol. Today *13*, 482–486.

Hatziapostolou, M., Polytarchou, C., Panutsopulos, D., Covic, L., and Tsichlis, P.N. (2008). Proteinase-activated receptor-1-triggered activation of tumor progression locus-2 promotes actin cytoskeleton reorganization and cell migration. Cancer Res. *68*, 1851–1861.

Heemskerk, J.W., Farndale, R.W., and SAGE, S.O. (1997). Effects of U73122 and U73343 on human platelet calcium signalling and protein tyrosine phosphorylation. Biochim. Biophys. Acta *1355*, 81–88.

Henkart, P.A. (1994). Lymphocyte-mediated cytotoxicity: two pathways and multiple effector molecules. Immunity *1*, 343–346.

Henkart, P.A., and Catalfamo, M. (2004). CD8+ effector cells. Adv. Immunol. *83*, 233–252.

Heuberger, D.M., and Schuepbach, R.A. (2019). Protease-activated receptors (PARs): mechanisms of action and potential therapeutic modulators in PAR-driven inflammatory diseases. Thromb. J. *17*, 4.

Hickman, H.D., Reynoso, G.V., Ngudiankama, B.F., Cush, S.S., Gibbs, J., Bennink, J.R., and Yewdell, J.W. (2015). CXCR3 chemokine receptor enables local CD8(+) T cell migration for the destruction of virus-infected cells. Immunity *42*, 524–537.

Hu, J.K., Kagari, T., Clingan, J.M., and Matloubian, M. (2011). Expression of chemokine receptor CXCR3 on T cells affects the balance between effector and memory CD8 T-cell generation. Proc. Natl. Acad. Sci. U S A *108*, E118–E127.

Hung, D.T., Wong, Y.H., Vu, T.K., and Coughlin, S.R. (1992). The cloned platelet thrombin receptor couples to at least two distinct effectors to stimulate phosphoinositide hydrolysis and inhibit adenylyl cyclase. J. Biol. Chem. *267*, 20831–20834.

Hurley, A., Smith, M., Karpova, T., Hasley, R.B., Belkina, N., Shaw, S., Balenga, N., Druey, K.M., Nickel, E., Packard, B., et al. (2013). Enhanced effector function of CD8(+) T cells from healthy controls and HIV-infected patients occurs through thrombin activation of protease-activated receptor 1. J. Infect. Dis. *207*, 638–650.

Intlekofer, A.M., Takemoto, N., Wherry, E.J., Longworth, S.A., Northrup, J.T., Palanivel, V.R., Mullen, A.C., Gasink, C.R., Kaech, S.M., Miller, J.D., et al. (2005). Effector and memory CD8+ T cell fate coupled by T-bet and eomesodermin. Nat. Immunol. *6*, 1236–1244.

Ishihara, H., Zeng, D., Connolly, A.J., Tam, C., and Coughlin, S.R. (1998). Antibodies to protease-activated receptor 3 inhibit activation of mouse platelets by thrombin. Blood *91*, 4152–4157.

Jenkins, M.R., and Griffiths, G.M. (2010). The synapse and cytolytic machinery of cytotoxic T cells. Curr. Opin. Immunol. *22*, 308–313.

Jin, J., Mao, Y., Thomas, D., Kim, S., Daniel, J.L., and Kunapuli, S.P. (2009). RhoA downstream of G(q) and G(12/13) pathways regulates protease-activated receptor-mediated dense granule release in platelets. Biochem. Pharmacol. *77*, 835–844.

Joshi, N.S., Cui, W., Chandele, A., Lee, H.K., Urso, D.R., Hagman, J., Gapin, L., and Kaech, S.M. (2007). Inflammation directs memory precursor and short-lived effector CD8(+) T cell fates via the graded expression of T-bet transcription factor. Immunity *27*, 281–295.

Ju, S.T., Cui, H., Panka, D.J., Ettinger, R., and Marshak-Rothstein, A. (1994). Participation of target Fas protein in apoptosis pathway induced by CD4+ Th1 and CD8+ cytotoxic T cells. Proc. Natl. Acad. Sci. U S A *91*, 4185–4189.

Kaech, S.M., and Cui, W. (2012). Transcriptional control of effector and memory CD8+ T cell differentiation. Nat. Rev. Immunol. *12*, 749–761.

Kaech, S.M., and Wherry, E.J. (2007). Heterogeneity and cell-fate decisions in effector and memory CD8+ T cell differentiation during viral infection. Immunity *27*, 393–405.

Kahn, M.L., Nakanishi-Matsui, M., Shapiro, M.J., Ishihara, H., and Coughlin, S.R. (1999). Protease-activated receptors 1 and 4 mediate activation of human platelets by thrombin. J. Clin. Invest. *103*, 879–887.

Kahn, M.L., Zheng, Y.W., Huang, W., Bigornia, V., Zeng, D., Moff, S., Farese, R.V.,, JR., Tam, C., and Coughlin, S.R. (1998). A dual thrombin receptor system for platelet activation. Nature *394*, 690–694.

Khoufache, K., Berri, F., Nacken, W., Vogel, A.B., Delenne, M., Camerer, E., Coughlin, S.R., Carmeliet, P., Lina, B., Rimmelzwaan, G.F., et al. (2013). PAR1 contributes to influenza A virus pathogenicity in mice. J. Clin. Invest. *123*, 206–214.

Klages, B., Brandt, U., Simon, M.I., Schultz, G., and Offermanns, S. (1999). Activation of G12/G13 results in shape change and Rho/Rho-kinase-mediated myosin light chain phosphorylation in mouse platelets. J. Cell Biol. *144*, 745–754.

Klenerman, P., and Zinkernagel, R.M. (1998). Original antigenic sin impairs cytotoxic T lymphocyte responses to viruses bearing variant epitopes. Nature *394*, 482–485.

Kumari, S., Curado, S., Mayya, V., and Dustin, M.L. (2014). T cell antigen receptor activation and actin cytoskeleton remodeling. Biochim. Biophys. Acta *1838*, 546–556.

Kurachi, M., Kurachi, J., Suenaga, F., Tsukui, T., Abe, J., Ueha, S., Tomura, M., Sugihara, K., Takamura, S., Kakimi, K., and Matsushima, K. (2011). Chemokine receptor CXCR3 facilitates CD8(+) T cell differentiation into short-lived effector cells leading to memory degeneration. J. Exp. Med. *208*, 1605–1620.

Lam, F.W., Vijayan, K.V., and Rumbaut, R.E. (2015). Platelets and their interactions with other immune cells. Compr. Physiol. *5*, 1265–1280.

Lazarevic, V., and Glimcher, L.H. (2011). T-bet in disease. Nat. Immunol. *12*, 597–606.

Le, V.B., Riteau, B., Alessi, M.C., Couture, C., Jandrot-Perrus, M., Rheaume, C., Hamelin, M.E., and Boivin, G. (2018). Protease-activated receptor 1 inhibition protects mice against thrombin-dependent respiratory syncytial virus and human metapneumovirus infections. Br. J. Pharmacol. *175*, 388–403.

Lee, P.R., Johnson, T.P., Gnanapavan, S., Giovannoni, G., Wang, T., Steiner, J.P., Medynets, M., Vaal, M.J., Gartner, V., and Nath, A. (2017). Protease-activated receptor-1 activation by granzyme B causes neurotoxicity that is augmented by interleukin-1beta. J. Neuroinflammation *14*, 131.

Leist, T., Althage, A., Haenseler, E., Hengartner, H., and Zinkernagel, R.M. (1989). Major histocompatibility complex-linked susceptibility or resistance to disease caused by a noncytopathic virus varies with the disease parameter evaluated. J. Exp. Med. *170*, 269–277.

Lopez, M.L., Soriano-Sarabia, N., Bruges, G., Marquez, M.E., Preissner, K.T., Schmitz, M.L., and Hackstein, H. (2014). Expression pattern of protease activated receptors in lymphoid cells. Cell Immunol. *288*, 47–52.

Lowin, B., Hahne, M., Mattmann, C., and Tschopp, J. (1994). Cytolytic T-cell cytotoxicity is mediated through perforin and Fas lytic pathways. Nature *370*, 650–652.

Lui-Roberts, W.W., Stinchcombe, J.C., Ritter, A.T., Akhmanova, A., Karakesisoglou, I., and Griffiths, G.M. (2012). Cytotoxic T lymphocyte effector function is independent of nucleus-centrosome dissociation. Eur. J. Immunol. *42*, 2132–2141.

Mari, B., Imbert, V., Belhacene, N., Far, D.F., Peyron, J.F., Pouyssegur, J., Van Obberghen-Schilling, E., Rossi, B., and Auberger, P. (1994). Thrombin and thrombin receptor agonist peptide induce early events of T cell activation and synergize with TCR cross-linking for CD69 expression and interleukin 2 production. J. Biol. Chem. *269*, 8517–8523.

McCoy, K.L., traynelis, S.F., and Hepler, J.R. (2010). PAR1 and PAR2 couple to overlapping and distinct sets of G proteins and linked signaling pathways to differentially regulate cell physiology. Mol. Pharmacol. *77*, 1005–1015.

McGavern, D.B., Christen, U., and Oldstone, M.B. (2002). Molecular anatomy of antigen-specific CD8(+) T cell engagement and synapse formation in vivo. Nat. Immunol. *3*, 918–925.

Migueles, S.A., Osborne, C.M., Royce, C., Compton, A.A., Joshi, R.P., Weeks, K.A., Rood, J.E., Berkley, A.M., Sacha, J.B., Cogliano-Shutta, N.A., et al. (2008). Lytic granule loading of CD8+ T cells is required for HIV-infected cell elimination associated with immune control. Immunity *29*, 1009–1021.

Monks, C.R., Freiberg, B.A., Kupfer, H., Sciaky, N., and Kupfer, A. (1998). Three-dimensional segregation of supramolecular activation clusters in T cells. Nature *395*, 82–86.

Mudd, J.C., Panigrahi, S., Kyi, B., Moon, S.H., Manion, M.M., Younes, S.A., Sieg, S.F., Funderburg, N.T., Zidar, D.A., Lederman, M.M., and Freeman, M.L. (2016). Inflammatory function of CX3CR1+ CD8+ T cells in treated HIV infection is modulated by platelet interactions. J. Infect. Dis. *214*, 1808–1816.

Ngai, J., Methi, T., Andressen, K.W., Levy, F.O., Torgersen, K.M., Vang, T., Wettschureck, N., and Tasken, K. (2008). The heterotrimeric G-protein alpha-subunit Galphaq regulates TCR-mediated immune responses through an Lck-dependent pathway. Eur. J. Immunol. *38*, 3208–3218.

Niessen, F., Schaffner, F., Furlan-Freguia, C., Pawlinski, R., Bhattacharjee, G., Chun, J., Derian, C.K., Andrade-Gordon, P., Rosen, H., and Ruf, W. (2008). Dendritic cell PAR1-S1P3 signalling couples coagulation and inflammation. Nature *452*, 654–658.

Oehen, S., Hengartner, H., and Zinkernagel, R.M. (1991). Vaccination for disease. Science *251*, 195–198.

Otani, H., Yoshioka, K., Nishikawa, H., Inagaki, C., and Nakamura, T. (2011). Involvement of protein kinase C and RhoA in protease-activated receptor 1-mediated F-actin reorganization and cell Growth in rat cardiomyocytes. J. Pharmacol. Sci. *115*, 135–143.

Pearce, E.L., Mullen, A.C., Martins, G.A., Krawczyk, C.M., Hutchins, A.S., Zediak, V.P., Banica, M., Dicioccio, C.B., Gross, D.A., Mao, C.A., et al. (2003). Control of effector CD8+ T cell function by the transcription factor Eomesodermin. Science *302*, 1041–1043.

Potter, T.A., Grebe, K., Freiberg, B., and Kupfer, A. (2001). Formation of supramolecular activation clusters on fresh ex vivo CD8+ T cells after engagement of the T cell antigen receptor and CD8 by antigen-presenting cells. Proc. Natl. Acad. Sci. U S A *98*, 12624–12629.

Radulovic, M., Yoon, H., Wu, J., Mustafa, K., and Scarisbrick, I.A. (2016). Targeting the thrombin receptor modulates inflammation and astrogliosis to improve recovery after spinal cord injury. Neurobiol. Dis. *93*, 226–242.

Ramachandran, R., Noorbakhsh, F., Defea, K., and Hollenberg, M.D. (2012). Targeting proteinase-activated receptors: therapeutic potential and challenges. Nat. Rev. Drug Discov. *11*, 69–86.

Rohani, M.G., Dijulio, D.H., An, J.Y., Hacker, B.M., Dale, B.A., and Chung, W.O. (2010). PAR1- and PAR2-induced innate immune markers are negatively regulated by PI3K/Akt signaling pathway in oral keratinocytes. BMC Immunol. *11*, 53.

Sambrano, G.R., Weiss, E.J., Zheng, Y.W., Huang, W., and Coughlin, S.R. (2001). Role of thrombin signalling in platelets in haemostasis and thrombosis. Nature *413*, 74–78.

Scholz, M., Vogel, J.U., Hover, G., Prosch, S., Kotchetkov, R., Cinatl, J., Koch, F., Doerr, H.W., and Cinatl, J., JR. (2004). Thrombin induces Sp1-mediated antiviral effects in cytomegalovirus-infected human retinal pigment epithelial cells. Med. Microbiol. Immunol. *193*, 195–203.

Sen, P., Gopalakrishnan, R., Kothari, H., Keshava, S., Clark, C.A., Esmon, C.T., Pendurthi, U.R., and Rao, L.V. (2011). Factor VIIa bound to endothelial cell protein C receptor activates protease activated receptor-1 and mediates cell signaling and barrier protection. Blood *117*, 3199–3208.

Sharma, M., Merkulova, Y., Raithatha, S., Parkinson, L.G., Shen, Y., Cooper, D., and Granville, D.J. (2016). Extracellular granzyme K mediates endothelial activation through the cleavage of protease-activated receptor-1. FEBS J. *283*, 1734–1747.

Sharma, R., Waller, A.P., Agrawal, S., Wolfgang, K.J., Luu, H., Shahzad, K., Isermann, B., Smoyer, W.E., Nieman, M.T., and Kerlin, B.A. (2017). Thrombin-induced podocyte injury is protease-activated receptor dependent. J. Am. Soc. Nephrol. *28*, 2618–2630.

Shpacovitch, V., Feld, M., Bunnett, N.W., and Steinhoff, M. (2007). Protease-activated receptors: novel PARtners in innate immunity. Trends Immunol. *28*, 541–550.

Simon, M.M., Waring, P., Lobigs, M., Nil, A., Tran, T., Hla, R.T., Chin, S., and Mullbacher, A. (2000). Cytotoxic T cells specifically induce Fas on target cells, thereby facilitating exocytosis-independent induction of apoptosis. J. Immunol. *165*, 3663–3672.

Smyth, M.J., Kelly, J.M., Sutton, V.R., Davis, J.E., Browne, K.A., Sayers, T.J., and Trapani, J.A. (2001). Unlocking the secrets of cytotoxic granule proteins. J. Leukoc. Biol. *70*, 18–29.

Soh, U.J., Dores, M.R., Chen, B., and Trejo, J. (2010). Signal transduction by protease-activated receptors. Br. J. Pharmacol. *160*, 191–203.

Stanners, J., Kabouridis, P.S., Mcguire, K.L., and Tsoukas, C.D. (1995). Interaction between G proteins and tyrosine kinases upon T cell receptor.CD3-mediated signaling. J. Biol. Chem. *270*, 30635–30642.

Steinhoff, M., Buddenkotte, J., Shpacovitch, V., Rattenholl, A., Moormann, C., Vergnolle, N., Luger, T.A., and Hollenberg, M.D. (2005). Proteinase-activated receptors: transducers of proteinase-mediated signaling in inflammation and immune response. Endocr. Rev. *26*, 1–43.

Stinchcombe, J.C., Bossi, G., Booth, S., and Griffiths, G.M. (2001). The immunological synapse of CTL contains a secretory domain and membrane bridges. Immunity *15*, 751–761.

Stinchcombe, J.C., and Griffiths, G.M. (2007). Secretory mechanisms in cell-mediated cytotoxicity. Annu. Rev. Cell Dev. Biol. *23*, 495–517.

Stinchcombe, J.C., Majorovits, E., Bossi, G., Fuller, S., and Griffiths, G.M. (2006). Centrosome polarization delivers secretory granules to the immunological synapse. Nature *443*, 462–465.

Suidan, H.S., Bouvier, J., Schaerer, E., Stone, S.R., Monard, D., and Tschopp, J. (1994). Granzyme A released upon stimulation of cytotoxic T lymphocytes activates the thrombin receptor on neuronal cells and astrocytes. Proc. Natl. Acad. Sci. U S A *91*, 8112–8116.

Sutherland, M.R., Friedman, H.M., and Pryzdial, E.L. (2007). Thrombin enhances herpes simplex virus infection of cells involving protease-activated receptor 1. J. Thromb. Haemost. *5*, 1055–1061.

Tamzalit, F., Wang, M.S., Jin, W., Tello-Lafoz, M., Boyko, V., Heddleston, J.M., Black, C.T., Kam, L.C., and Huse, M. (2019). Interfacial actin protrusions mechanically enhance killing by cytotoxic T cells. Sci. Immunol. *4*, eaav5445.

Taqueti, V.R., Grabie, N., Colvin, R., Pang, H., Jarolim, P., Luster, A.D., Glimcher, L.H., and Lichtman, A.H. (2006). T-bet controls pathogenicity of CTLs in the heart by separable effects on migration and effector activity. J. Immunol. *177*, 5890–5901.

Tsun, A., Qureshi, I., Stinchcombe, J.C., Jenkins, M.R., de la Roche, M., Kleczkowska, J., Zamoyska, R., and Griffiths, G.M. (2011). Centrosome docking at the immunological synapse is controlled by Lck signaling. J. Cell Biol. *192*, 663–674.

van der Most, R.G., Murali-Krishna, K., Whitton, J.L., Oseroff, C., Alexander, J., Southwood, S., Sidney, J., Chesnut, R.W., Sette, A., and Ahmed, R. (1998). Identification of Db- and Kb-restricted subdominant cytotoxic T-cell responses in lymphocytic choriomeningitis virus-infected mice. Virology *240*, 158–167.

Van Gassen, S., Callebaut, B., Van Helden, M.J., Lambrecht, B.N., Demeester, P., Dhaene, T., and Saeys, Y. (2015). FlowSOM: using self-organizing maps for visualization and interpretation of cytometry data. Cytometry A *87*, 636–645.

Varma, R., Campi, G., Yokosuka, T., Saito, T., and Dustin, M.L. (2006). T cell receptor-proximal signals are sustained in peripheral microclusters and terminated in the central supramolecular activation cluster. Immunity *25*, 117–127.

Vouret-Craviari, V., Boquet, P., Pouyssegur, J., and Van Obberghen-Schilling, E. (1998). Regulation of the actin cytoskeleton by thrombin in human endothelial cells: role of Rho proteins in endothelial barrier function. Mol. Biol. Cell *9*, 2639–2653.

Vu, T.K., Hung, D.T., Wheaton, V.I., and Coughlin, S.R. (1991). Molecular cloning of a functional thrombin receptor reveals a novel proteolytic mechanism of receptor activation. Cell *64*, 1057–1068.

Waldman, A.D., Fritz, J.M., and Lenardo, M.J. (2020). A guide to cancer immunotherapy: from T cell basic science to clinical practice. Nat. Rev. Immunol. *20*, 651–668.

Wang, T., Lee, M.H., Choi, E., Pardo-Villamizar, C.A., LEE, S.B., Yang, I.H., Calabresi, P.A., and Nath, A. (2012). Granzyme B-induced neurotoxicity is mediated via activation of PAR-1 receptor and Kv1.3 channel. PLoS One *7*, e43950.

Wherry, E.J., Blattman, J.N., Murali-Krishna, K., van der Most, R., and Ahmed, R. (2003). Viral persistence alters CD8 T-cell immunodominance and tissue distribution and results in distinct stages of functional impairment. J. Virol. *77*, 4911–4927.

Wilson, T.J., Nannuru, K.C., and Singh, R.K. (2009). Cathepsin G recruits osteoclast precursors via proteolytic activation of protease-activated receptor-1. Cancer Res. *69*, 3188–3195.

Woulfe, D.S. (2005). Platelet G protein-coupled receptors in hemostasis and thrombosis. J. Thromb. Haemost. *3*, 2193–2200.

Wurzer, H., Hoffmann, C., Al Absi, A., and Thomas, C. (2019). Actin cytoskeleton Straddling the immunological synapse between cytotoxic lymphocytes and cancer cells. Cells *8*, 463.

Xu, W.F., Andersen, H., Whitmore, T.E., Presnell, S.R., YEE, D.P., Ching, A., Gilbert, T., Davie, E.W., and Foster, D.C. (1998). Cloning and characterization of human protease-activated receptor 4. Proc. Natl. Acad. Sci. U S A *95*, 6642–6646.

Yin, Y.J., Salah, Z., Grisaru-Granovsky, S., Cohen, I., Even-Ram, S.C., Maoz, M., Uziely, B., Peretz, T., and Bar-Shavit, R. (2003). Human protease-activated receptor 1 expression in malignant epithelia: a role in invasiveness. Arterioscler Thromb. Vasc. Biol. *23*, 940–944.

Yokosuka, T., Sakata-Sogawa, K., Kobayashi, W., Hiroshima, M., Hashimoto-Tane, A., Tokunaga, M., Dustin, M.L., and Saito, T. (2005). Newly generated T cell receptor microclusters initiate and sustain T cell activation by recruitment of Zap70 and SLP-76. Nat. Immunol. *6*, 1253–1262.

Yu, Y., Smoligovets, A.A., and Groves, J.T. (2013). Modulation of T cell signaling by the actin cytoskeleton. J. Cell Sci. *126*, 1049–1058.

Zhang, N., and Bevan, M.J. (2011). CD8(+) T cells: foot soldiers of the immune system. Immunity *35*, 161–168.

Zinkernagel, R.M., Haenseler, E., Leist, T., Cerny, A., Hengartner, H., and Althage, A. (1986). T cell-mediated hepatitis in mice infected with lymphocytic choriomeningitis virus. Liver cell destruction by H-2 class I-restricted virus-specific cytotoxic T cells as a physiological correlate of the 51Cr-release assay? J. Exp. Med. *164*, 1075–1092.

STAR★METHODS

KEY RESOURCES TABLE

REAGENT or RESOURCE	SOURCE	IDENTIFIER
Antibodies		
CD3	BD	Cat# 347344, RRID:AB_400286
CD8	Invitrogen	Cat# Q10009, RRID:AB_2556437
CD45RA	BioLegend	Cat# 304118, RRID:AB_493657
CD27	BD	Cat# 560222, RRID:AB_1645474
PAR1	Beckman Coulter	Cat# IM2584,RRID:AB_131066
CXCR3	BD	Cat# 561730, RRID:AB_10894207
Eomes	ThermoFisher	Cat# 51-4877-41, RRID:AB_1603272
Tbet	BD	Cat# 561267, RRID:AB_10564093
GZA	BioLegend	Cat# 507214, RRID:AB_2114395
GZB	BioLegend	Cat# 515405, RRID:AB_2294995
Perforin	ThermoFisher	Cat# 17-9994-41, RRID:AB_10853169
CD3	BD	Cat# 561389, RRID:AB_10679120
CD8	ThermoFisher	Cat# 95-0081, RRID:AB_1603266
CD4	ThermoFisher	Cat# 45-0042, RRID:AB_1107001
IFNγ	BD	Cat# 554413, RRID:AB_398551
TNFα	BD	Cat# 554418, RRID:AB_395379
IL2	BD	Cat# 554428, RRID:AB_395386
CD45.2	BD	Cat# 564616, RRID:AB_2738867
CD8	BD	Cat# 564920, RRID:AB_2716856
CD44	BD	Cat# 562464, RRID:AB_11153123
CD62L	BD	Cat# 560517, RRID:AB_1645210
CD127	BioLegend	Cat# 135010, RRID:AB_1937251
KLRG1	BioLegend	Cat# 38421, RRID:AB_2563800
CXCR3	BD	Cat# 562937, RRID:AB_2687551
CX3CR1	BioLegend	Cat# 149014, RRID:AB_2565698
CD27	BD	Cat# 565307, RRID:AB_2739173
CXCR4	BioLegend	Cat# 146517, RRID:AB_2687244
CD31	BioLegend	Cat# 102524, RRID:AB_2572182
CD69	BioLegend	Cat# 104525, RRID:AB_10683447
CD107a	BD	Cat# 564349, RRID:AB_2738762
IFNγ	BD	Cat# 554413, RRID:AB_398551
TNFα	BD	Cat# 554418, RRID:AB_395379
Chemicals, peptides, and recombinant proteins		
LCMV gp31-41	Anaspec	AS-61669
SCH530348	Bio-techne/Tocris	
SCH79797	Axon Medchem	Axon 1275
U73122	Sigma, MO	CAS 112648-68-7
U73343	Sigma, MO	142,878-12-4
Critical commercial assays		
Pan ToxiLux substrate	OncoImmunin	
NFL1	OncoImmunin	

(*Continued on next page*)

Continued

REAGENT or RESOURCE	SOURCE	IDENTIFIER
FLIPR calcium 4 assay kit	Molecular Devices	R8142
CD8 negative selection kit	Miltenyi Biotech	130-094-156
Cell Trace™ Far Red	Thermo Fisher/Invitrogen	C34572
Experimental models: Organisms/strains		
B6.129S4-*F2r*^{tm1Ajc}/J	Jackson Laboratory	002,862
SJL Cd45a(Ly5a)/Nai	Taconic Biosciences	4007
Software and algorithms		
FlowJo software	BD Biosciences	
GraphPad prism	GraphPad	

RESOURCE AVAILABILITY

Lead contact

Further information and requests for resources and reagents should be directed to and will be fulfilled by the lead contact, Dr. Marta Catalfamo (mc2151@georgetown.edu).

Materials availability

This study did not generate new unique reagents.

Data and code availability

This paper does not report original code. Data reported in this paper will be shared by the lead contact upon request. Any additional information required to reanalyze the data reported in this paper is available from the lead contact upon request.

EXPERIMENTAL MODEL AND SUBJECT DETAILS

Human CD8 T cell isolation and culture

Healthy controls were obtained from healthy volunteers (both male and female, ages range from 35 to 70) at the NIH-Blood Bank. Healthy donors were consented and studied under IRB approved protocol. Human peripheral blood mononuclear cells (PBMC) from 10 healthy donors were collected and stained for PAR1, T-bet, Eomes, GZA, GZB, perforin and CXCR3, as well as CD45RA and CD27 for T cell subsets identification. PBMCs from healthy controls (n = 10) were obtained by Ficoll gradient centrifugation and CD8 T cells were isolated using negative selection (Miltenyi Biotech, Auburn, CA), resuspended at 2 × 10^6 cells/mL in X-VIVO 15 medium (Lonza, NJ) and activated with plate bound mAbs CD3/CD28 (10 μg/mL and 5 μg/mL respectively, BD Biosciences, CA). After 3 days of culture, activated CD8 T cells were re-adjusted at a concentration of 2 × 10^6 cells/mL in X-VIVO 15 with 50 U/mL rhIL-2 (TECIN, National Cancer Institute, Frederick, MD) and cultured for another 11–18 days.

Mice

PAR1$^{-/-}$ mouse line (B6.129S4-*F2r*^{tm1Ajc}/J) was established using embryos purchased from the Jackson Laboratory. PAR1$^{-/-}$ P14 mouse strain was generated by crossbreeding PAR1$^{-/-}$ mice with P14 (B6 Thy1.1^{+}D^{b}GP$_{33–41}$ TCR-tg) mice. Recipient mice B6.SJL Cd45a(Ly5a)/Nai were purchased from Taconic Biosciences. All mice were bred and maintained under specific pathogen-free conditions at the National Institute of Health (NIH) animal facilities. Animal experimental procedures were conducted in accordance with the guidelines and proposal approved by NIH Animal Care and Use Committee. Male and female mice between 6 and 12 weeks old were used for *in vivo* experiments.

EXPERIMENTAL MODEL AND SUBJECT DETAILS

Methods details

Calcium flux assay. 0.3 × 10^6 cells/well of activated CD8 T cells were resuspended in Ca^{2+} buffer (HBSS + Ca^{2+} + Mg^{2+} + 1 mg/mL BSA+ 20 mM HEPES) and mixed with an equal volume of component A (FLIPR Calcium 4 assay kit, Molecular Devices, CA) in a 96-well plate. After 30 min of incubation at 37°C and 5% CO_2,

media or the PAR1 inhibitors SCH530348 (Bio-techne/Tocris, MN) and SCH79797 (Axon Medchem, VA), PLC inhibitor U73122 and its analog U73343 (Sigma, MO) were added to the cells and they were further incubated another 20 min. The plate was then centrifuged (2 min, 900 rpm) and the Calcium assay was performed with a FlexStation 3 plate reader (Molecular Devices, CA). The Ca^{2+} responses induced by 1 μg/mL anti-CD3 mAb were analyzed for 30–200 s. Ca^{2+} responses to PAR agonists peptides were performed using 100 μM of PAR1 (TFLLR-NH2), PAR2 (SLIGRL-NH2), PAR4 (AY-NH2), and PAR1 control peptide (RLLFT-NH2). The data were exported to a text file (with WinMDI). The graphs were generated with Prism. The data were exported to a text file (with WinMDI). The graphs were generated with Prism.

RT-qPCR analysis. qPCR was performed to determine mRNA expression of PARs in resting human and murine CD8 T cells. RNA from CD8 T cells were extracted with TRIzol reagent (Invitrogen CA). RNA was then reversed transcribed into cDNA. Primers used: Human PAR1 (NM_010,169.3): forward, 5′-ATGAAAGCGT CCTGCTGGAG-3′; reverse, 5′-GGACGTTCAGAGGAAGGCTG-3′; human PAR2 (NM_007,974.4): forward, 5′-GCTGGGAGGTATCACCCTTCT-3′; reverse, 5′-CGCAGAGAACTCATCGATGGA-3′; human PAR3 (NM_010,170.4): forward, 5′-TGCCAGTCACTGTTTGCCAA-3′; reverse, 5′-CTCGGGACACTCCGCTTTTAT-3′; human PAR4 (NM_007,975.3): forward, 5′-GACCCCCAGCATCTACGATG-3′; reverse, 5′-CAGCAGCAGTGCTT GAGAGCT-3′; murine PAR1 (NM_001,992.3): forward, 5′-CAAATGCCACCTTAGATCCCC-3′; reverse, 5′-CG GAGGCATCTTCTGAGATGA-3′; murine PAR2 (NM_005,242.4): forward, 5′-AGCCTCTCTCTCCTGCAG TGG-3′; reverse, 5′-GCAAACCCACCACAAACACA-3′; murine PAR3 (NM_001,256,566.1): forward, 5′-AGAC CTTTCGTGGAGCTCCC-3′; reverse, 5′-AACACCA:GGAGGTAGATGGCA-3′; murine PAR4 (NM_003,950.2): forward, 5′-GGTGCCCGCCCTCTATGG-3′; reverse, 5′-CCGCGAGGTTCATCAGCA-3′.

Redirected killing assay and degranulation experiments. Cytotoxicity assay measures the delivery of GZB inside the target cells as shown by fluorescence signal of the GZB substrate and upstream caspase activities to the target cells. Granule exocytosis is measured by surface expression of CD107a on human CD8 effector cells.

FAS^{-}L1210 were stained with 0.2 mM Cell Trace Far Red (Thermo Fisher/Invitrogen, MA). Cell were biotinylated with 0.2 mM biotin (EMD, MO) followed by incubation with 0.02 mg/mL streptavidin (MilliporeSigma, MO). FAS^{-}L1210 and activated CD8 T cells from healthy controls were labeled with NFL1 (OncoImmunin, MD) for exclusion of death cells before the experiment. For PAR1 blockade, activated CD8 T cells were pre-incubated for 20 min at 37°C and 5% CO_2 with media, or SCH79797 (2.5 μM, 5 μM, Bio-techne/Tocris, MN), SCH530348 (10 μM, 20 μM, 40 μM, Axon Medchem, VA), U73122 (1 μM, Millipore Sigma, MO), or U73343 (1 μM, Millipore Sigma, MO). Cells were mixed with FAS^{-} L1210 at 27:1 effector to target ratio in the presence or absence of anti-CD3 mAb.

For cytotoxicity experiments: The pre-treated activated CD8 T cells were stimulated 1 h with media or 10 ug/mL anti-CD3 biotin (eBioscience, CA) in the presence of 4× Pan ToxiLux substrate (OncoImmunin, MD) and 3.7×10^4 L1210 at 37°C and 5% CO_2. Following the stimulation CD8 T cells were collected, washed and acquired using FACS LSRII and analyzed with FlowJo software (BD Biosciences, CA).

For degranulation assays: Pre-treated activated CD8 T cells were stimulated 1 h with media or 10 μg/mL anti-CD3 biotin in the presence of 0.25×10^6 L1210 at 37°C and 5% CO_2. Following the stimulation CD8 T cells were stained 30 min at 4°C with anti-CD8 (SK1, BD Biosciences, CA) and anti-CD107a (H4A3, BD Biosciences, CA) then acquired using FACS LSRII and analyzed with FlowJo software (BD Biosciences, CA).

Murine CD8 T cell functional assays. naive P14 CD8 T cells were isolated from P14 (B6 $Thy1.1^{+}D^{b}GP_{33–41}$ TCR-tg) mice using negative selection from lymph nodes of WT or $PAR1^{-/-}$ mice. Feeder cells were prepared using total splenic cells from naive WT mice that underwent 2500 rads irradiation. P14 cells were cocultured with feeder cells in the presence of 1 μg/mL GP33 peptide for two days, followed by 3 days in culture with IL-2 (50 U/mL).

Mouse lymphoma cell line EL4 was used as target cells for degranulation and cytotoxicity assays. For degranulation experiments, EL4 cells were pulsed with various concentration of GP33 peptide (0, 10^{-6}, 10^{-4}, 10^{-2} and 1 μg/mL) for one hour at 37°C and 5% CO_2. *In vitro* activated WT or $PAR1^{-/-}$ CD8 T cells were cocultured with pulsed targets at 1:1 ratio for 60 min at 37°C and 5% CO_2. CD107a (Clone 1D4B, BD Biosciences, CA) and monensin (2 nM, Biolegend, CA) were added before the incubation. Cells were

washed and stained for 20 min at 4°C with antibodies against CD3 (Clone 17A2) and CD8 (Clone 53.6.7). Dead cells were labeled with propidium iodide shortly before flow cytometry analysis and surface CD107a expression was measured as indication for degranulation of CD8 T cells.

For cytotoxicity assay, EL4 cells were labeled with 0.2 μM Cell Trace Far Red dye (Invitrogen, CA) for 8 min at 37°C and 5% CO_2. Cells were washed and pulsed with 1 μg/mL GP33 peptide for another 1 h. NFL1 (OncoImmunin, MD) was used to stain dead cells of EL4 targets and CD8 effector cells. Cells were then cocultured at E:T ratio of 9:1 and 3:1 for 45 min in the presence of GranToxiLux substrate (OncoImmunin, MD) at 37°C and 5% CO_2. After incubation, cells were washed and kept cold for flow cytometry analysis.

Microscopy. FAS^{-}L1210 target cells were biotinylated as described above. Activated human CD8 T cells were pre-incubated 20 min with or without SCH79797 (5 μM, Bio-techne/Tocris, MN) before mixing with the FAS^{-}L1210 at 1:1 E:T ratio. Conjugates using murine T cells were performed using as targets the EL4 cell line pulsed with 1 μg/mL GP33 peptide for 1 h. Conjugates were made by coculturing EL4 cells with activated WT or PAR1$^{-/-}$ P14 CD8 T cells for 20 min. Cells were allowed to adhere to poly-L-lysine-coated coverslips for 30 min and were fixed with 4% PFA for 60 min, quenched twice with 50 mM NH_4Cl for 5 min, permeabilized with 1% NP40, and then stained with Phalloidin (Cell Signaling, MA) and alpha-tubulin antibody (DM1A, Cell Signaling, MA) to visualize actin architecture and the microtubule-organizing center (MTOC) localization. Coverslips were mounted with Prolong with DAPI (Invitrogen, CA). Stained conjugates were imaged using DeltaVision Elite deconvolution microscopy with 60X oil immersion objective. Integrated intensity of Phalloidin staining at the immunological synapse was calculated using ImageJ and MetaMorph software. MTOC was characterized as distal, proximal and docked to the immunological synapse.

LCMV infection. PAR1$^{-/-}$ and WT littermates were intravenously infected with 2 × 10^5 pfu of LCMV WE 2.5 strain. Mice were sacrificed and perfused after six or eight days, and spleen and liver were collected for immune phenotype and T cell function analysis using flow cytometry. Serum was collected and viral titer was determined by plaque assay.

For adoptive cell transfer experiments 10^4 naive CD8 T cells purified from lymph node of WT or PAR1$^{-/-}$ P14 mice by negative selection were transferred intravenously into B6.SJL Cd45a(Ly5a)/Nai recipient mice respectively. One day later, mice were infected with 10^5 PFU of LCMV WE 2.5 stain. T cell phenotype and cytokine production were analyzed at day 6 or 8 post infection. For cytokine production, splenic and liver cells were restimulated *in vitro* with 1 μg/mL GP33 peptide (LCMV gp31-41, KAVYNFATM, Anaspec, CA) in the presence of 5 μg/mL of Brefeldin A and 50 U/mL IL2. Cells were stained with surface markers including CD3 (Clone 17A2), CD8 (Clone 53–6.7), CD45.2 (Clone 104), CXCR3 (Clone CXCR3-173), CX3CR1 (Clone SA011F11) and CD27 (Clone LG.3A10). Cells were then washed and stained intracellularly using antibodies against IFNγ (Clone XMG1.2) and TNFα (Clone MP6-XT22). Antibodies were listed in supplemental tables. Cells were acquired by BD FACS LSRII or Symphony flow cytometer and analyzed using FlowJo 10 software (BD Biosciences, CA).

Adoptive co-transfer of WT and PAR1$^{-/-}$ P14 CD8 T cells. 5000 P14 CD8 T cells were purified from lymph node of WT (B6.P14.CD45.2Thy1.1) and PAR1$^{-/-}$ (B6.P14.CD45.2Thy1.2) mice respectively and adoptively co-transferred (i.v.) into CD45.1.Thy1.2 recipient mice. Recipient mice were infected the next day with LCMV WE 2.5 strain (2 × 10^5 pfu, i.v). Six days post infection, splenic and liver cells were isolated and *in vitro* stimulated with LCMV GP33 peptides for 4 h. Phenotype, cytokine production and degranulation were analyzed.

FlowSOM analysis. Multidimensional single cell analysis was performed using FlowSOM algorithm (Flow Self Organizing Map, FlowJo). To generate FlowSOM map, we concatenated 10^5 manually gated CD8 T cells from spleen and liver of each WT and PAR1$^{-/-}$ mouse of the adoptive transfer experiments and apply the map to each condition to allow unsupervised clustering of CD8 T cells. Maps were generated based on seven selected surface and intracellular markers: IFNγ, TNFα, CD107a, CXCR3, CX3CR1, CD27 and CD45.2.

QUANTIFICATION AND STATISTICAL ANALYSIS

Statistical analysis was performed by GraphPad prism software using non-parametric paired Wilcoxon test or Mann-Whitney U test. p value <0.05 was considered significant.